JOURNAL OF QUATERNARY SCIENCE (2024) **39**(5) 710–728 ISSN 0267-8179. DOI: 10.1002/jqs.3620

JQS Journal of Quaternary Science QRA Quaternary Research Association

Mineral magnetism and palaeoenvironment recorded in loess in southern England

DOMINIKA NIEZABITOWSKA,[1,2]* THOMAS STEVENS,[1,3] BALÁZS BRADÁK,[4] MARTIN CHADIMA,[5,6] YUNUS BAYKAL,[1] DANIELE SECHI[7] and RAMONA SCHNEIDER[1]

[1]Department of Earth Sciences, Uppsala, Uppsala University, Sweden
[2]Institute of Geophysics Polish Academy of Sciences, Warsaw, Poland
[3]Department of Geosciences and Geography, University of Helsinki, Helsinki, Finland
[4]Department of Maritime Sciences, Kobe, Kobe University, Japan
[5]AGICO, Brno, Czech Republic
[6]Institute of Geology of the Czech Academy of Sciences, Prague, Czech Republic
[7]Department of Architecture, Design and Planning, University of Sassari, Alghero (SS), Italy

Received 7 February 2024; Revised 21 March 2024; Accepted 2 April 2024

ABSTRACT: Extensive research has focused on the loess deposits in southern England, aiming to unravel their stratigraphic and palaeoenvironmental significance. However, no systematic mineral magnetic study on these deposits has yet been undertaken. Here we address this by investigating the magnetic mineral composition and alignment of loess at two sites in southern England, Lowland Point (LP) on the Lizard Peninsula of Cornwall, and Pegwell Bay (PB) in eastern Kent on the Isle of Thanet. A set of rock magnetic analyses was conducted to understand mineral magnetism within the studied sections. In addition, the primary depositional origin of the magnetic fabrics as well as their overprinting caused by various possible post-depositional processes were examined through anisotropy of magnetic susceptibility (AMS). The magnetic mineral composition is similar at both sites, derived from both sedimentary (aeolian) and post-depositional processes. The AMS results show magnetic foliation that varies between the two sites, aligning with the bedding plane, indicating deposition from gravitational dust fall at the PB site, and a stronger wind transport energy at the LP site. Although the magnetic lineation of bulk AMS is relatively weak, there is a noticeable tendency towards alignment in most samples, with flow directions from the SE indicated at both sections if a strong wind is assumed at LP, although with a possible SW direction if a weaker wind is assumed. These observations may imply the preservation of palaeowind directions during dust transport, with a substantial southerly component, which contradicts previous assertions of dominant northerly or northeasterly winds. Indeed, a possible dominant southeasterly wind direction between 25 and 18 ka would suggest a limited influence of katabatic, westerly or polar northeasterly winds during dust transport, and rather may imply the effect of low-pressure systems passing through the English Channel during that period. © 2024 The Authors *Journal of Quaternary Science* Published by John Wiley & Sons Ltd

KEYWORDS: anisotropy of magnetic susceptibility; loess deposition; magnetic composition; nanofabric; palaeowind

Introduction

Thin loess deposits of up to c. 4 m thickness cover significant parts of southern Britain (Figure 1) (Catt et al., 1987; Lehmkuhl et al., 2021; Bunce et al., 2022). These predominantly late Quaternary deposits (Wintle, 1981, Stevens et al., 2020) have long been studied but considerable uncertainty exists over their source, formation and relevance for understanding past climate change (e.g. Eden, 1980; Smalley et al., 2009; Baykal et al., 2022). Indeed, a recently published review of loess in Britain and Ireland (Bunce et al., 2022) highlights uncertainty over the distribution and formation of true loess (*sensu lato*; the terrestrial accumulation of windblown dust, dominantly silt, with clays and fine sand particles), which currently limits its use in understanding past environmental changes and landscape processes of southern Britain and NW Europe more widely. Furthermore, notwithstanding a few multi-proxy investigations suggesting valuable palaeoclimate information is preserved within loess deposits in southern England (as evident in studies by Rose et al., 2000; Stevens et al., 2020), the utilization of such records remains limited. One key question is the extent to which loess deposits in Britain are reworked by processes such as gelifluction, hydro-consolidation, cryoturbation and pedoturbation (e.g. Clarke et al., 2007; Milodowski et al., 2015; Butcher, 1990), or whether primary airfall deposits are preserved. Moreover, loess facies are highly variable across southern Britain, and reworking of loess is probably highly site-specific, and linked to local topography and conditions (Bunce et al., 2022).

Mineral magnetism is widely used in studies of loess deposits, to understand past climate, landscape and post-depositional reworking conditions (e.g. Oches & Banerjee, 1996; Költringer et al., 2021a, 2021b; Bradák, 2009; Bradák et al., 2011). In particular, the magnetic susceptibility of loess, and its frequency dependence, is widely used as a proxy for past soil formation. However, the controls on the magnetic susceptibility signal in loess can be complex (e.g. Bradák et al., 2021), especially for loess in peri- or paraglacial environments (Marković et al., 2012; Bunce et al., 2022), and additional rock magnetic experiments such as hysteresis, remnant magnetism or temperature dependence are required

*Correspondence: Dominika Niezabitowska, as above.
Email: dominika.niezabitowska@geo.uu.se

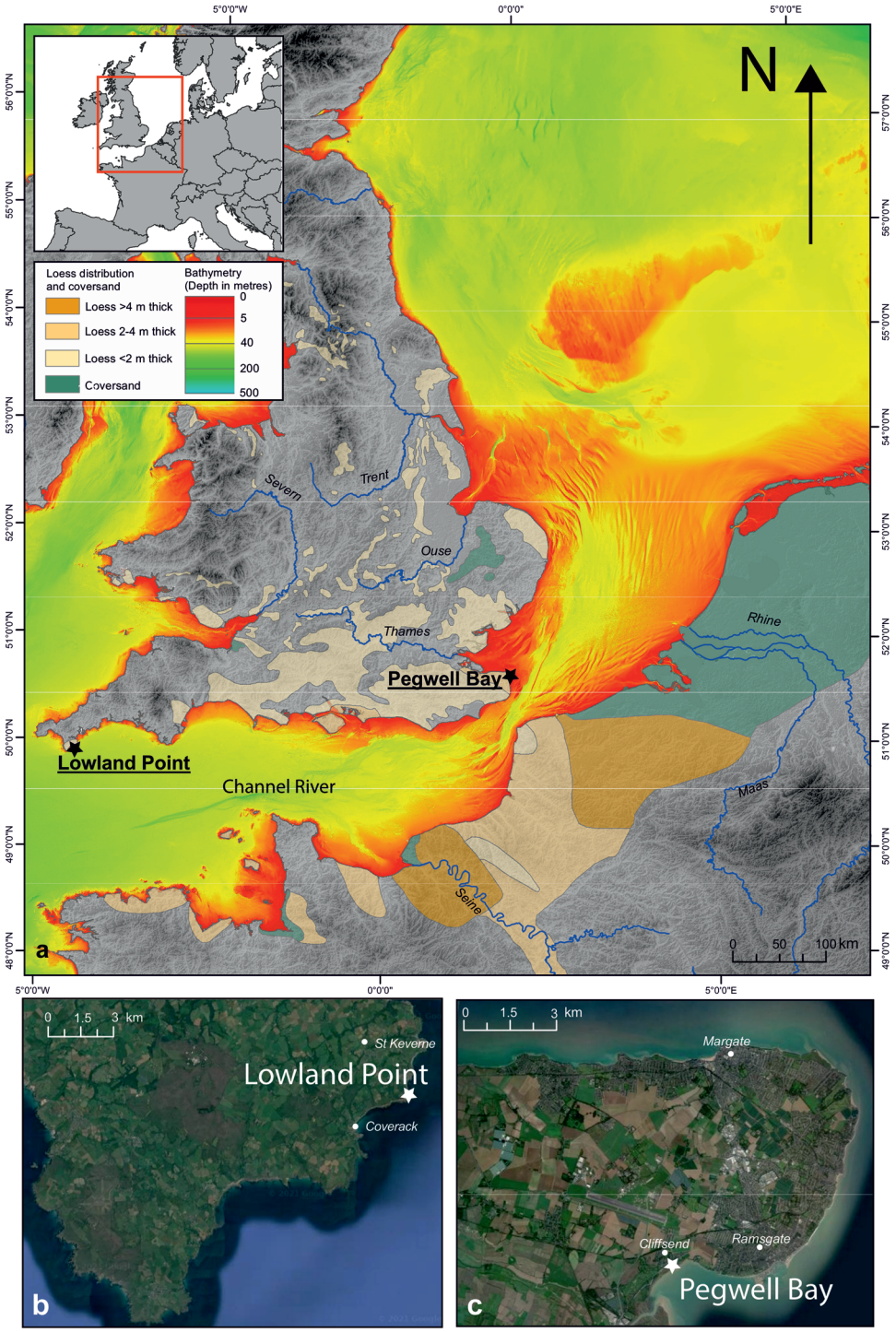

Figure 1. (a) Map of southern Britain and English Channel area loess and coversand deposits, topography and bathymetry, with sample sites marked and zoom in around (b) Lowland Point and (c) Pegwell Bay. Modified from Stevens et al. (2020) with loess thickness based on Catt (1977), Antoine et al. (2003) and Bateman & Catt (2007). [Color figure can be viewed at wileyonlinelibrary.com]

to fully understand the controls on iron oxide mineral type and grain sizes in loess (e.g. Hus, 2003; Lagroix and Banerjee, 2002; Liu et al., 2005; Necula et al., 2015; Taylor et al., 2014; Gao et al., 2019; Költringer et al., 2021a, 2021b; and references therein). Furthermore, to reconstruct depositional conditions and post-depositional reworking, magnetic fabric has been determined by applying anisotropy of magnetic susceptibility (AMS) measurements, and in ideal cases may be used for palaeowind reconstruction (e.g. Thistlewood and Jianzhong, 1991; Bradák et al., 2018; Költringer et al., 2021b).

As long as it is not extensively reworked, examining the ice-marginal loess preserved in southern Britain using AMS, therefore, offers an opportunity to reconstruct the impact of extensive ice sheets on atmospheric circulation over Europe. However, despite the widespread use of these techniques across European loess (e.g. Bradák et al., 2021), the mineral magnetism of loess in Britain has not yet been studied in detail and only two early studies have utilized AMS to attempt to understand depositional and reworking processes in loess in southern England (Butcher, 1990) and close by NW France (Derbyshire & Mellors, 1988). Butcher (1990) argued that slope movement had extensively reworked loess across Britain under an 'aqueous' or 'solifluction' regime, dominantly originating from higher ground to the north. Derbyshire & Mellors (1988) suggested that the reworking of loess in

northern France and southern Britain was evidenced by anisotropy grain alignment in scanning electron microscopy analysis of thin sections and laser scanning of grains and that anisotropic fabrics in northern French loess confirmed this. However, it is now known that anisotropic magnetic fabrics shown in AMS analysis are not necessarily the result of reworking (e.g. Nawrocki et al., 2006; Bradák et al., 2021). Furthermore, there is mixed evidence for the reworking of loess in southern Britain, with some studies reporting *in situ* deposits (Rose et al., 2000; Stevens et al., 2020), others showing mixed *in situ* and reworked (Milodowski et al., 2015), and others arguing for extensive or near complete reworking, i.e. through periglacial activity (e.g. Antoine et al., 2003). Furthermore, little specific detail on the evaluation and interpretation of AMS data in Derbyshire & Mellors (1988) is presented, while Butcher (1990) is an unpublished PhD thesis, which makes it hard to assess the reproducibility and implications of these findings and interpretations.

Stevens et al. (2020) performed some preliminary rock magnetic experiments on loess at Pegwell Bay (PB) in east Kent and found a mixture of single-domain (SD) and multi-domain (MD, or PSD – pseudo-single-domain) magnetic grains, with the dominant magnetic mineral carrier being magnetite, similar to other loess deposits globally (e.g. Lagroix and Banerjee, 2002; Liu et al., 1992; Pan et al., 2002; Jin and Liu, 2010; Li et al., 2018; Taylor et al., 2014; Necula et al., 2015). However, Stevens et al. (2020) found only limited evidence of weathering and control of superparamagnetic (SP) grains on increased magnetic susceptibility in soils. Instead, they concluded that the 'wind-vigour' model of magnetic enhancement (see e.g. Chlachula et al., 1998) may be appropriate for part of the section, while pedogenetic or hydromorphic dissolution models (Baumgart et al., 2013; Taylor et al., 2014; Bradák, 2009; Bradák et al., 2011) may be more applicable over other intervals. Furthermore, evidence from temperature-dependent magnetic susceptibility experiments suggested that neoformation of maghaemite as coatings on larger MD magnetite grains may have occurred due to weak pedogenesis at certain intervals in the sequence (see e.g. Spassov et al., 2003; Hao et al., 2009; to compare); thus, the magnetic mineralogy in loess at PB is complex and with potentially multiple competing influences.

Overall then, previous work on loess in Britain using rock magnetic analysis hints at a complex picture, but has focused only on one site and misses some methods that may further elucidate the controls on mineral magnetism. Furthermore, AMS analysis of loess in Britain has been extremely limited, and considerable uncertainty still exists over whether the deposits preserve depositional fabrics. Here we attempt to overcome these limitations by conducting a detailed rock magnetic analysis of two contrasting loess sections in the far east and west of southern England (Figure 1): Thanet, Kent (PB), and Lizard Peninsula (Lowland Point, LP), Cornwall, respectively. We apply routine magnetic susceptibility and frequency-dependent susceptibility analyses, together with a range of rock magnetic experiments, and conduct preliminary AMS and frequency-dependent AMS analyses of pilot samples from the two sections. The AMS investigation aims primarily to ascertain if undisturbed depositional fabrics are present in the loess, and subsequently to provide initial hints at the specific near-surface winds responsible for transporting dust over NW Europe during the Last Glacial Maximum (LGM). These proposed regimes include a high-pressure cell over the European Ice Sheet (EIS) with easterly winds (Schaffernicht et al., 2020), cyclones tracking over the channel (Antoine et al., 2009) or prevailing katabatic winds (Lefort et al., 2013a).

Sites and study areas

The loess section at PB (51°19.651′N, 001°22.200′ E) is located at the eastern edge of the Isle of Thanet (eastern Kent) and exposed at the sea cliffs of PB at Cliffs End (Figure 1), the site of a former hover port. Here the sequence unconformably overlies the late Palaeocene shallow marine sands of the Thanet Formation (Stevens and Baykal, 2021) or heavily brecciated upper Cretaceous chalk (Pitcher et al., 1954). The site was first studied by White (1928) and named as loess by Pitcher et al. (1954) and Kerney (1965). It was later dated in detail using quartz optically stimulated luminescence (OSL) by Clarke et al. (2007) and Stevens et al. (2020), the latter showing that the majority of the loess was deposited between 25 and 18 ka. The 3.3-m-thick loess sequence is capped by a grey to brown modern/Holocene soil, below which lies a non-calcareous blocky brownish loess. Underlying this, an abrupt boundary marks the transition to calcareous yellow loess with faint brown banding in the upper part and sandy bands towards the base (Figure 2). The interpretation of many of these stratigraphic features is still debated, and a detailed stratigraphy is presented in Stevens et al. (2020) who argue that permafrost active layer freeze–thaw processes drive the stratigraphic changes between the two main loess units. Loess on Thanet is some of the thickest in Britain, and at least the lower loess unit is buff-coloured and calcareous, and has a porous, open structure that is reminiscent of more 'classical' loess deposits in Eastern Europe and Asia. However, in general, there is no consensus about the degree of reworking of the Thanet loess deposits (Catt et al., 1987; Clarke et al., 2007; Milodowski et al., 2015; Stevens et al., 2020). Recent detailed multi-method provenance analysis of loess at PB reveals that it comprises British–Irish Ice Sheet (BIIS)-derived dust, via glaciofluvial systems in the exposed North Sea (Baykal et al., 2022). However, given that these ice sheet-derived materials were probably transported by glaciofluvial systems over a wide area, this leaves the question of past dust-transporting wind directions open.

By contrast, loess deposits at LP (50°02.205′ N, 005°04.141′ W, Figure 1), belonging to the Lizard Loess Formation (Roberts, 1985), are non-calcareous and much darker (Figure 2). The main section (LP2019) crops out on a low, flat promontory consisting of Devonian gabbro backed by a raised beach terrace (Budge, 1842) and a palaeocliff line, and is located c. 2.5 km NE of Coverack on the eastern edge of the Lizard Peninsula (west Cornwall). Underlying the c. 1.8-m-thick loess is a unit of geliflucted loessic material with extensive angular gabbro clasts (Ealey and James, 2011). Below the thin O horizon of the modern soil is a c. 30-cm-thick darker grey silt that has occasionally rounded clasts and has previously yielded Mesolithic flint flakes and cores, as well as pottery sherds (Dawson, 2013) (Figure 2). This layer is underlain by a unit of stone-free dark silt, mostly dark brown in colour but with irregular orange and lighter brown streaks, bands and tongues. At the base of this unit (down to c. 1.1 m), a weak frost wedge was identified, penetrating into the unit below, which comprises banded loess down to 1.6 m (Figure 2). The bands are alternating dark, finer-grained, and lighter, coarser-grained (sandier) bands c. 0.5–1 cm thick, and are similar to banded loess described in northern France and Jersey (Lautridou, 1985; Antoine et al., 2003), termed *limon á doublet* (Lautridou & Sommé, 1974, Derbyshire & Mellors, 1988; Keen et al., 1996; Bunce et al., 2022). While the origin of these features is controversial, they have been interpreted to indicate permafrost processes ('tounged' horizon, frost wedge) and freezing and thawing cycles of seasonal snow melt-inducing low-energy overland flow

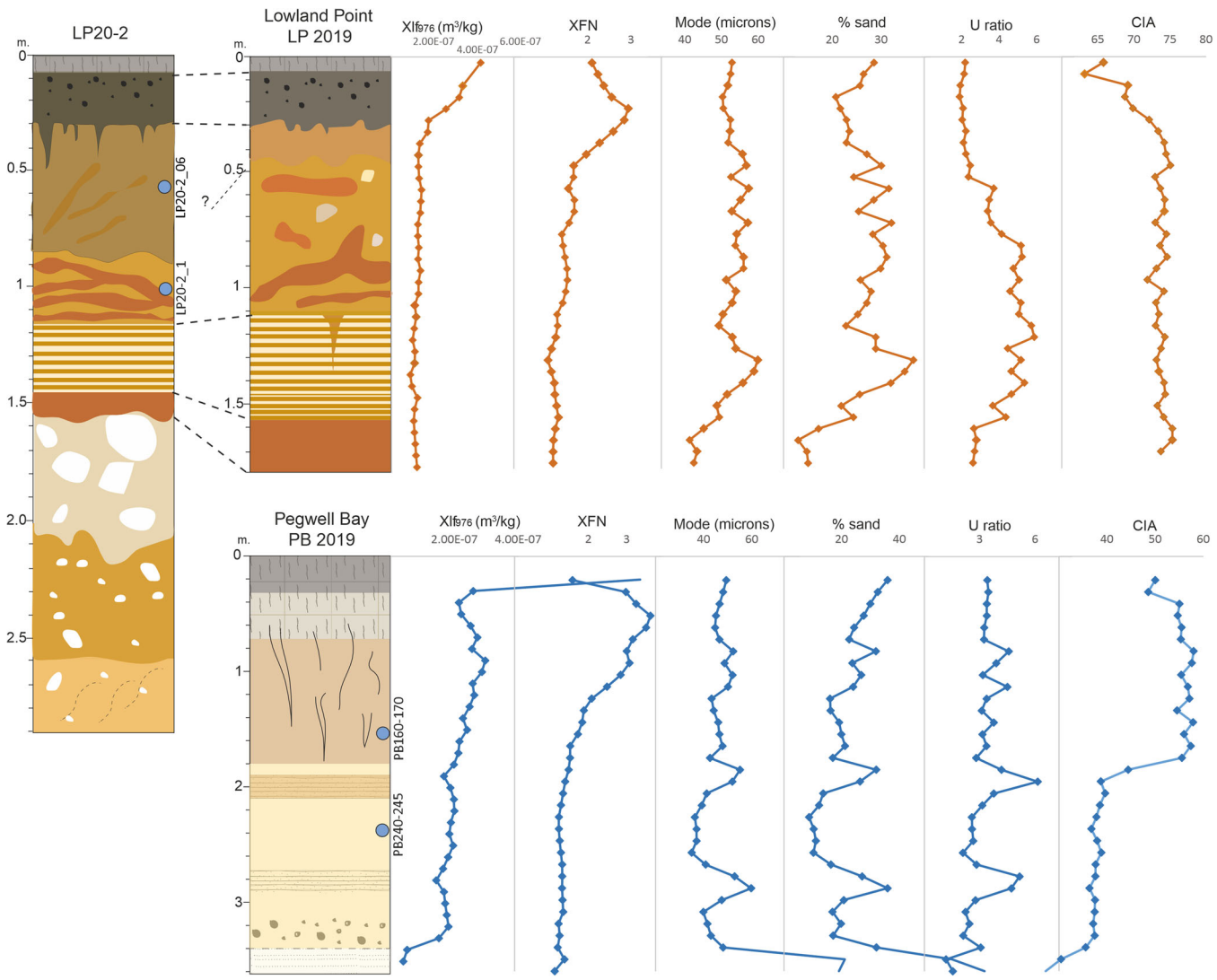

Figure 2. Stratigraphy, magnetic susceptibility, grain size and selected geochemical proxies of the sample sites by depth. Stratigraphy is described in the text. Abbreviations: χlf_{976} and χFN, low-frequency (976 Hz) and frequency-dependent magnetic susceptibility, respectively. The U-ratio is calculated after Vandenberghe and Nugteren (2001). CIA, chemical index of alteration (see Supporting Information for details). Blue dots on stratigraphic charts represent the depth of AMS samples. Note that the majority of samples from Lowland Point were taken from LP 2019 but AMS samples are from LP20-2. Stratigraphic correlation is based on visual stratigraphy in the field. [Color figure can be viewed at wileyonlinelibrary.com]

(*limon á doublet*) (Haesaerts et al., 1981; Derbyshire & Mellors, 1988). Underlying the banded loess is a darker, compacted silt that overlies the gelifluction deposits (Figure 2), which are better exposed at section LP20-2, c. 5–10 m to the SE. Section LP20-2 shows a similar loess stratigraphy to the LP2019 section, albeit with a noticeably darker upper part of the loess below the upper soil (Figure 2). The loess at LP has been examined previously by a number of authors, including Catt and Staines (1982), Roberts (1985), Ealey and James (2011) and Scott et al. (2011), while Wintle (1981) first applied thermoluminescence dating to a single sample from the site, suggesting loess deposition around 16 ka.

LP is one of the main loess exposures of the Lizard Loess Formation (Roberts, 1985), which comprises a gelifluctedlower unit and an apparently *in situ* aeolian upper loess (Ealey and James, 2011). Immediately to the east in Devon, the loess is generally thinner, while in Cornwall it thickens, with the thickest deposits found on the serpentinite and gabbro of the Lizard Peninsula (Catt and Staines, 1982). The reasons for the remarkable association of Lizard Loess with certain bedrock types, as well as its unusual thickness, are unclear, although local sources and permeability of underlying bedrock may be factors (Catt and Staines, 1982; Ealey and James, 2011).

In addition to the permafrost features in the loess at LP discussed above, Ealey and James (2008) argue that the irregular contact between the upper structureless loess and the lower gelifluctedloess exhibits periglacial involutions or periglacial-driven fragipan formation. Indeed, sporadic last glacial permafrost features have been identified over the whole of Cornwall (James, 2004).

Sampling and methods

Samples were taken from a cleaned exposed cliff section at PB and freshly dug sections in the low cliffs at LP. Non-oriented samples were taken at regular 5- to 10-cm intervals at all sites, while flat lying c. 10-cm-thick blocks of loess were cut and oriented to the north (two each from PB and LP20-2 section) at representative depths in the exposed sections (Figure 2). At PB the loess was sufficiently compact and cemented such that complete blocks could be cut by knife from the section. At LP, the soft and less consolidated nature of the sediments meant that blocks were cut with a knife with the help of a plastic container, to keep the sampled blocks intact after sampling.

A detailed description of methods can be found in the Supporting Information.

Results

Magnetic susceptibility, grain size and geochemistry by depth

Absolute low-frequency (976 Hz) magnetic susceptibility (χlf) values are similar at the two sites, with slightly higher values in the upper unit at LP (Figure 2). Frequency-dependent magnetic susceptibility (χFN) values are low at both sites, mostly <3%. At both sites, the χ parameters decrease with depth, although at LP this happens more rapidly in the uppermost part of the profile, and χFN values form peaks in the upper soils, with the uppermost values decreasing again to the surface. Peak values in χlf and χFN do not exactly match but broadly coincide with the Holocene soil. Grain-size parameters are also similar at both sites (Figure 2), although larger abrupt changes are seen at PB and coincide with sandier layers and at the boundary with the underlying Thanet Formation. Sand content also increases in the banded loess at LP. Modes are generally in the coarse silt range at both sites. In the banded loess of the LP site, the U-ratio decreases significantly (from values c. 5 to c. 2) at c. 0.8–0.5 m, while in contrast at PB higher U-ratios occur in coarser bands (at 2.0 and 2.8 m depths), reaching values up to 6 (Figure 2). The chemical index of alteration (CIA) at PB is dominated by the transition from calcareous to non-/weakly calcareous loess at c. 1.8 m, but generally values are lower than those at LP (Figure 2). The CIA drops slightly in the upper c. 0.3 m at LP. Similarly, the Rb/Sr ratio is probably influenced by the dynamics of carbonates in the PB section, but generally higher values of Rb/Sr in the LP section suggest more intensive weathering and pedogenesis (see Supporting Information Fig. S1). In turn, the chemical proxy of alteration, insensitive for uncertainties in separating carbonate-Ca from silicate-Ca or from biases due to K-fixation (e.g. illitization of smectite) (see Buggle et al., 2011), shows higher values in the LP section (84 – 92) than the PB section (from 47 m in the lower part, up to 70 in the upper one) (see Fig. S1). As expected, the values of pedogenic indicators, such as CIA and Rb/Sr, are higher in the LP section and the upper part of the PB site, and the quotients $(CaO^* + Na_2O + MgO)/TiO_2$ and Na_2O/Al_2O_3 are in line with this observation (Fig. S1).

Magnetic domain characteristics

The ratio of coercivity of remanence (remanent coercive force) to coercivity (Hcr/Hc) falls into the range of approximately 1.2–6 for LP samples, with an average concentrated around 4 and a standard deviation of 0.9. The average Hcr/Hc ratio for PB samples is slightly lower (3.62) with a much lower standard deviation (0.44) compared to LP. The ratio of saturation remanence to saturation magnetization (Mrs/Ms) ranges from approximately 0.1 to 0.23 for all specimens (Figure 3). Despite the larger scatter in the LP data, the average of Mrs/Ms ratio for both specimen groups is 0.12, with a slightly higher standard deviation for LP (0.03) than for PB (0.01). Most of the samples are located in the PSD region of the Day plot. Based on the study of Dunlop (2002), the PSD region represents a mixed MD and SD grain size character, which, in the case of the studied samples, indicates a mixture of c. 80–90% MD and 10–20% SD grains. Some exceptional specimens show higher, c. 40–50%, SD content. The majority of the specimens tend to move toward the region of the MD + SD mixing curve, and interestingly, no SP domain character can be convincingly identified (Figure 3a). Complementing the results of the Day plot, most of the specimens fall into the MD region in the Tauxe plot with a possible appearance of mixed uniaxial single domain (USD) + SP component (Figure 3b).

Thermomagnetic characteristics

The most common feature among all types of heating curves is a clear decrease of magnetization at about 550–600 °C (Fig. S2a–h). In contrast to the recent soil samples from both sites, which are quasi-demagnetized following this drop (Fig. S2a, b and e), the loess samples still have residual magnetization which disappears when the temperature reaches c. 660–700 °C (Figs S2c, d, f–h). Along those common characteristics, there are also some features of the heating curves which are characteristic for particular groups of specimens. Some curves from the LP loess specimens show a significant inflection or bump between c. 120 and 200 °C (Fig. S2c and d). Similar inflection points or bumps were

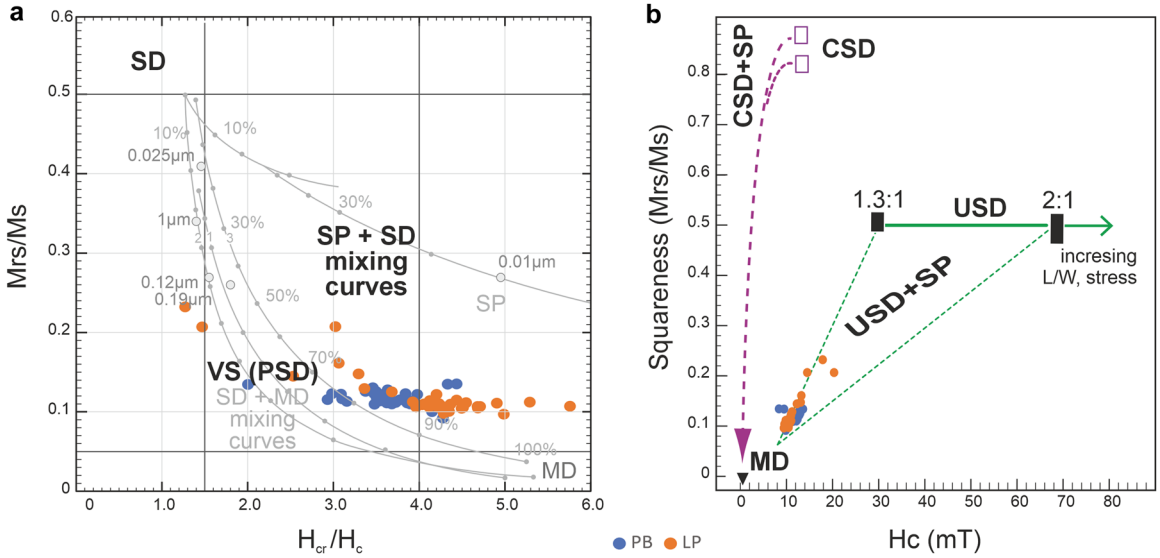

Figure 3. Magnetic domain (grain size) characteristics of the magnetic contributors in the studied sections. (a) Day plot (Day et al., 1977; Dunlop, 2002) and (b) Tauxe plot (Tauxe et al., 2002). Abbreviations: USD, uniaxial single domain (grains that can be magnetized in only one of two directions, thus showing uniaxial anisotropy); MD, multi-domain; SP, superparamagnetic; SD, single domain; PSD, pseudo-single domain; VS, vortex state (e.g. Roberts et al., 2017); L, length; W, width. [Color figure can be viewed at wileyonlinelibrary.com]

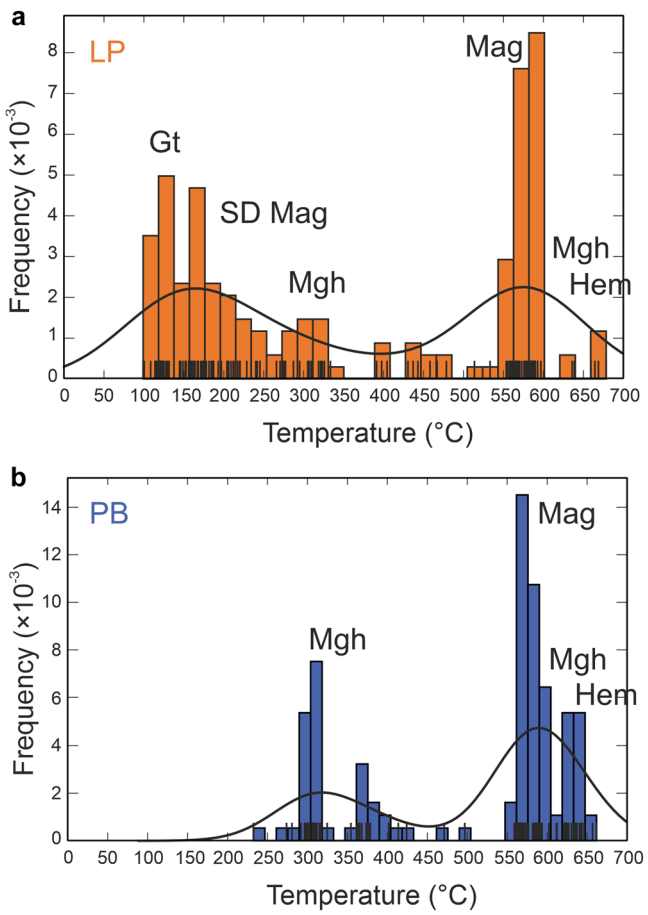

Figure 4. The distribution and probability of inflection points appearing during heating experiments of the selected samples from LP and PB (LP: 36 and PB: 32). The plot combines a histogram, a rug-plot which indicates every observation by a small vertical tick and the results of kernel density estimation (KDE). Abbreviations: Gt, goethite; Hem, haematite; (SD) Mag, (single-domain) magnetite; Mgh, maghaemite. [Color figure can be viewed at wileyonlinelibrary.com]

observed in specimens from the lower, calcareous loess unit of the PB profile between c. 250 and 400 °C (Fig. S2g and h). A relatively unique double peak feature from loess sections appears between ~300 and 500 °C in the surface soil samples (Fig. S2a, b and e).

The frequency of various inflection points in the samples is shown in Figure 4. In general, the following main characteristic group of inflection points are indicated by the kernel density estimation (KDE) in the heating curves during the thermomagnetic experiments: one at ~100–230 °C (LP section; Figure 4a), one between ~250 and 450 °C (appears in LP but is characteristic in the PB section; Figure 4b), and another one between ~550 and 650 °C (both LP and PB sections; Figure 4). The histograms show more details, in comparison to the thermomagnetic curves. The ~100–220 °C bump in the KDE of LP consists of two significant inflection points, one at c. 150 °C, and a group of inflection points between c. 180 and 220 °C (Figure 4a). Significant numbers of the thermomagnetic curves contain an inflection point between ~250 and 450 °C (appears in LP but mainly in the PB section). As already suggested above, the most characteristic inflection points of the thermomagnetic curves are located around 550–600 °C (both in LP and PB samples; Figure 4). At around 630–650 °C, some additional inflection points were observed mainly in the PB section.

All samples display a Verwey transition on room-temperature saturation isothermal remanent magnetization (RT-SIRM) and low-temperature saturation isothermal remanent magnetization (LT-SIRM) curves (Fig. S5). However, in both zero field cooling (ZFC) and field cooling (FC) curves the transition is hardly visible (Fig. S5), which may suggest titanium substitution or a grain size effect (for further discussion see 'Magnetic mineral composition of the loess' below). The transition occurs at ~110–115 K [–163.15 to –158.15 °C], which suggests a small degree of cation deficiency, probably modified by maghaemitization (after Özdemir et al., 1993). FC SIRM has a higher intensity than a ZFC LT-SIRM suggesting SD magnetite (Carter-Stiglitz et al., 2006). The RT-SIRM curves present a decrease of remanence during warming to 400 K (126.85 °C), which suggests reaching the Néel temperature (TN) (Fig. S5b–d; see Özdemir & Dunlop, 1996). Higher values of FC ZFC remanences and increasing differences between them while cooling confirm the occurrence of goethite grains (Fig. S5; after Özdemir and Dunlop, 1996; Liu et al., 2006). The Morin transition was not observed (Fig. S5).

Generally, in all specimens, ZFC and FC remanences decrease with increasing temperature with no distinct drops (Fig. S5a and c, see 'Magnetic mineral composition of the loess' below for further discussion). The rapid decrease in intensity below 60 K and then a more gradual decrease to 300 K can be attributed to typical superparamagnetic behaviour and is consistent with the presence of SP grains and/or decreasing magnetocrystalline anisotropy in phases like goethite (e.g. Banerjee et al. 1993; Moskowitz et al., 1993; Passier & Dekkers 2002).

Thermal and field dependence of magnetic susceptibility

The magnetic susceptibility variations in the temperature (κT) provide very similar results to the thermomagnetic analyses. The most common feature among the heating curves is a clear decrease at about 550–600 °C (Fig. S3), suggesting the presence of magnetite. Other common features are the inflection points or bumps between c. 250 and 400 °C and a characteristic peak around ~500 °C (Fig. S3). The latter peak can be recognized in the cooling curve as well. Similar to the results of the thermomagnetic experiments from the surface soil samples (Fig. S2a, b and e), this may also be interpreted as a double peak feature, appearing between ~300 and 500 °C. In the case of the κT experiments, the phenomenon appears in loess samples as well (Fig. S3). Less common features are the inflection or bump between c. 120 and 200 °C, and the small bump between c. 650 and 700 °C, which appears in PB170 (Fig. S3). The low-temperature κT curves show one inflection point at approximately –160 to –150 °C (c. 120 K), characteristic for the Verwey transition (T_V), indicating the presence of magnetite in most of the presented samples, especially visible in PB samples (Fig. S3).

There are significant differences between the initial and final susceptibility values of the samples, particularly the LP samples and PB210. Together with the irreversible heating and cooling cycles, this possibly indicates ferromagnetic mineral (e.g. magnetite or haematite) neoformation from paramagnetic components (e.g. clay minerals) during the heating experiments (see e.g. Ao et al., 2009).

Both LP20_2_1_4 and PB240-245_17 specimens show relatively weak susceptibility with a slight increase (c. 1%) in magnetic susceptibility as a function of field (Fig. S4). No obvious differences in the trends are seen between samples or applied measurement frequencies.

Anisotropy of magnetic susceptibility – examination of pilot samples

While all of the measurements passed the F-test (Jelínek, 1977), 64 of the 74 measurements show statistically significant magnetic lineation with $F12 > 4$ and $\varepsilon 12 < 20°$ (statistical

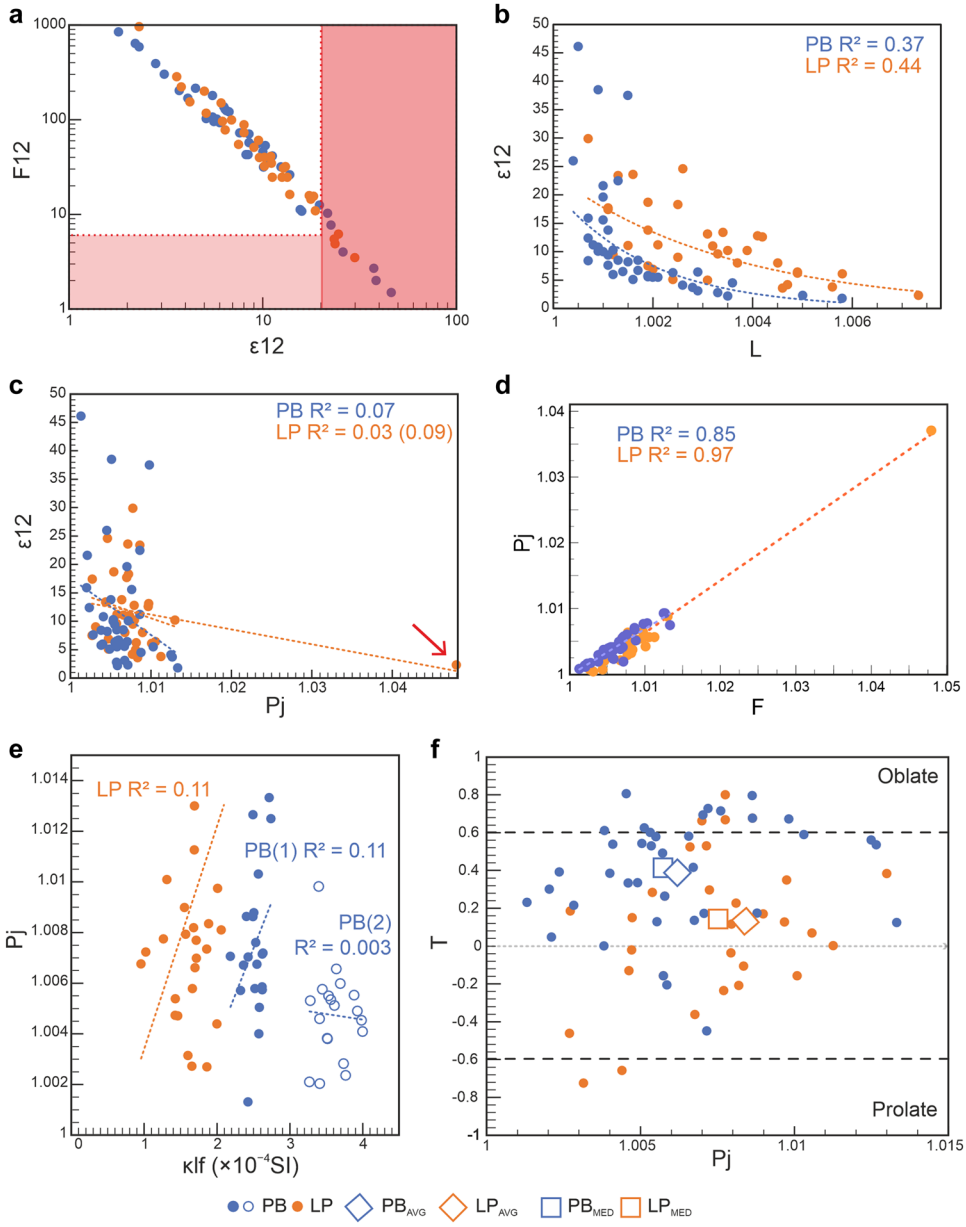

Figure 5. Evaluation of the magnetic fabric parameters by various methods following Lagroix and Banerjee (2004) and Zhu et al. (2004). Plots reveal the relationship between various magnetic parameters, such as (a) ε_{12} and *F12* (samples located in the pink area were excluded from the analysis); (b) lineation (*L*) and ε_{12}; (c) corrected degree of anisotropy (*Pj*) and ε_{12}; (d) examination of the potential influence of paramagnetic contributors on the magnetic fabric [*Pj* vs. foliation (*F*)], following the method of Rochette et al. (1992) and Taylor and Lagroix (2015); (e) characterization of the magnetic fabric of the samples by the Jelinek plot (see Supporting Information and 'Discussion of AMS results and their environmental interpretation' for further information about the plots); and (f) *Pj* vs. shape parameter of AMS ellipsoid (*T*). Note that samples from PB are separated: sample PB160-170 (open circles) and sample PB240-245 (filled circles) on plot (e). [Color figure can be viewed at wileyonlinelibrary.com]

parameters described in the SM) and 61 samples had well-resolved foliation (*F23* > 10) (Figure 5, Table S1) following Zhu et al. (2004) and Lagroix and Banerjee (2004). *ε12* shows an inverse relationship to lineation (*L*) in the case of both the LP and PB samples. There is a slight difference between the magnetic fabric parameters of LP and PB samples. The distribution of PB specimens is similar to those presented in Lagroix and Banerjee (2004), indicating a lower variation of κ_{max}, compared to the scattering of maximum principal susceptibility axi (κ_{max}) in LP samples (Figure 5b). No statistical relationship exists between *ε12* and corrected degree of anisotropy of magnetic susceptibility (*Pj*) (Figure 5c). The absence of a correlation between *Pj* and mean value of principal susceptibility axis (κ_{mean}) and strongly correlated foliation (*F*) with *Pj* ($r > 0.85$), as depicted in Figure 5, both imply that magnetic anisotropy is governed by the paramagnetic mineral fraction (which includes silicates and clays), rather than by ferrimagnetic minerals such as magnetite (e.g. Borradaile, 1987; Rochette et al., 1992; Hus, 2003; see 'Discussion of AMS results and their environmental interpretation' below for further discussion).

The allocation of the samples is scattered in the Jelinek plot, without forming any characteristic group (Figure 5f). In contrast to the PB samples, which are scattered around mainly the oblate–triaxial ($T > 0$) region of the plot, LP samples are located in the prolate–triaxial ($T < 0$) area as well. Although loess samples are often characterized by strongly oblate (planar), foliated fabric ($T > \sim 0.5$–0.6) only some samples fall into this region (mainly from the PB profile), and most of the samples are located in the triaxial region ($-0.5 < T < 0.5$).

Most of the samples' bulk magnetic fabrics indicate quasi-horizontal magnetic foliation, with magnetic lineation scattered on this foliation plane to varying extents (Figure 6b–d). The bulk magnetic fabric of the PB specimens seems to be more foliated

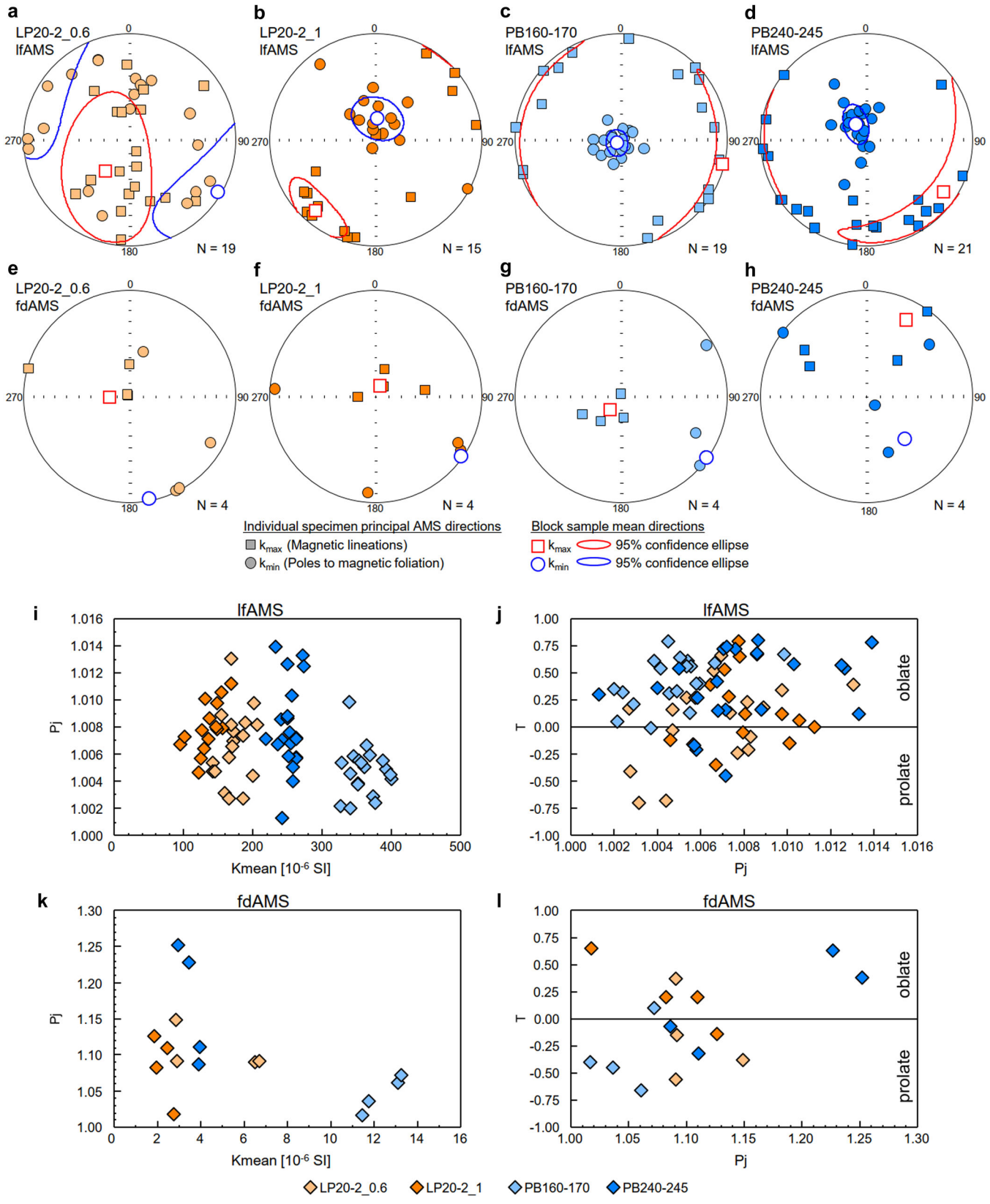

Figure 6. Bulk magnetic fabric and the separation of superparamagnetic fabric from the bulk magnetic fabric in pilot specimens from loess horizons of LP and PB successions. Stereoplots (a)–(d) present magnetic fabric measured at low frequency (976 Hz), representing the alignment of all magnetic contributors in the samples ('bulk magnetic fabric'). Squares represent K1 and circles represent K3 of each specimen, the confidence ellipses (red and blue lines), and mean tensor directions of the block sample (larger empty symbols). Stereoplots (e)–(h) show the orientation of the frequency-dependent magnetic components ('nanofabric') for each specimen with the mean tensor (empty symbols). The plots in the lower part present the relationships between AMS parameters: mean magnetic susceptibility and corrected degree of anisotropy of magnetic susceptibility (*Pj*) for bulk AMS (i) and fdAMS (k), and between *Pj* and shape parameter (*T*) for bulk (j) and fdAMS (l). [Color figure can be viewed at wileyonlinelibrary.com]

(compacted). However, the scattering of the orientation of the κ_{max} axis seems larger (Figure 6c and d) compared to the better-aligned but less foliated LP (Figure 6b). An exception to this is that the bulk magnetic fabric of LP20-2_06 has more scattered magnetic fabric compared to the other LP sample (Figure 6a). The above series of AMS measurements were focused on the general characterization of the magnetic fabric. In contrast, the separation of fabric by applied frequency (fdAMS) allows analysis of SP and SD frequency-dependent contributors (so-called 'nanofabric'). The alignment of the frequency-dependent contributors (fdAMS) seems to be different compared to the bulk AMS magnetic fabric in all samples. The 'nanofabric' of both LP samples and the upper layer of the PB site (Figure 6e–g) shows the vertical orientation of κ_{max} axes, probably implying inversed fdAMS fabric, normally typical for SD magnetite (see 'Site palaeoenvironmental comparison – Environmental magnetic approach' below for more details).

Discussion

Magnetic mineral composition of the loess

The magnetic domain size of loess at PB mainly falls into the PSD or mixed MD and SD region of the Day plot (Dunlop, 2002). In addition, some of the PB samples and a significant amount of LP samples are located in the MD region (Figure 3a). These results are similar to those of loess from Alaska (Lagroix and Banerjee, 2002), the Chinese Loess Plateau (e.g. Liu et al., 1992; Pan et al., 2002; Jin and Liu, 2010; Li et al., 2018), Europe and Russia (e.g. Taylor et al., 2014; Necula et al., 2015; Költringer et al., 2021b), and show that generally PSD (or mixed MD and SD state) and MD components are the main magnetic contributors in loess and soil units.

The clear drop in magnetization and susceptibility in the heating curves at about 550–600 °C, observed in almost all samples, indicates the Curie temperature (T_C) of magnetite or oxidized magnetite (Dunlop and Özdemir, 1997) (Figs S2a–h and S3). The T_V on RT-SIRM and LT-SIRM curves and heating curves of κT at ~120 K (−153.15 °C) confirms this conclusion (Figs S3 and S5). In all cases, the transition is not abrupt but rather extends across a temperature range of ten degrees or more. The suppression or masking of the Verwey transition can be attributed to several factors, including non-stoichiometry and/or cation substitution in magnetite crystals, or the effects of grain size (e.g. Kąkol & Honig, 1989; Özdemir et al., 1993). The dominance of magnetite in the studied samples is reinforced by the weakly positive field dependence (Fig. S4; max. 1.5%), which hints at the dominance of MD magnetite (e.g. Worm et al., 1993; Jackson et al., 1998; Hrouda et al., 2006), and is also consistent with the low χFN in the samples (see Figure 2 and S4).

Small amounts of high-temperature residual magnetization, disappearing gradually up to 680–700 °C, may indicate the presence of haematite (T_C of haematite: 680 °C), especially in the PB profile. However, haematite observed in high-temperature experiments can be an end product of magnetite and/or maghaemite alteration in elevated (>450 °C) temperatures (see Krs et al., 1992; Tarling and Hrouda, 1993; Deng et al., 2001). This conclusion is in line with the lack of an observed Morin transition, characteristic for haematite in low-temperature measurements (Fig. S5). Note that this does not exclude the presence of ultrafine-grained haematite, if any (see Jiang et al., 2014 for details). However, even a small amount of impurities in SP haematite grains may have a significant influence on magnetization, which might suppress or mask the transition (Jiang et al., 2014).

The bump observed at ~120 °C in LP loess samples (Figure 4a and S2) and the PB170 sample (Fig. S2) may indicate two different contributors. The inflection around 120 °C (Figure 4a) as well as the decrease of magnetization on the RT-SIRM curve while heating to 400 K (126.85 °C, Fig S5) may indicate the Néel temperature of goethite (Özdemir and Dunlop, 1996). This feature may overlap with the slight increase in magnetisation from room temperature to about 200 °C, and the rapid intensity decrease of FC SIRM below 60 K (see Fig. S5a and c) probably reflecting the unblocking of SD particles (e.g. Liu et al., 2005; Moskowitz et al., 1993). This suggests that the LP and PB samples contain ultrafine pedogenic ferrimagnetic grains of size near the SP/stable single domain (SSD) boundary (the size of the magnetite grains is around 10–25 nm; Dearing et al., 1996), in line with fdAMS results (see Figure 6e–g). However, the Day and Tauxe plot did not yield conclusive evidence of SP components (as depicted in Figure 3). Additionally, χFN indicates low values (>1%) in the lower part of the profile and slightly higher values (around 3%) in the upper part of the LP section, implying a very limited (if any) presence of SP particles (see Figure 2, and 'Anisotropy of magnetic susceptibility – examination of pilot samples' above for more detailed insights). This distinction can be attributed to the proposition put forth by Buggle et al. (2014), suggesting the preferential degradation of fine-grained magnetic particles in lower layers due to excess moisture or waterlogging. These apparently contradictory findings point to possible limitations of various magnetic methods in the study of loess–palaeosol sequences with complex, mixed magnetic mineral assemblages.

The bump observed in PB loess samples between c. 250 and 400 °C can be explained by the appearance of various contributors (Figure 4b and S3). In particular, it may indicate the thermally induced transformation of metastable maghaemite (γ-Fe_2O_3) (Gendler et al., 2005; Liu et al., 2010; Gao et al., 2019). Alternatively, the small step or bump may indicate the alteration of iron sulphides [e.g. pyrrhotite ($Fe_{(1-x)}S$) or pyrite (FeS_2)] to iron oxides during heating (Schneider et al., 2004; Sagnotti, 2007), although these are not common mineral contributors in loess.

A relatively unusual asymmetric double peak feature between ~300 and 500 °C from both loess sections, observed in the surface of soil samples, may indicate the two stages of mineral transformation: conversion of lepidocrocite to maghaemite, and later to haematite (see e.g. Gehring and Hofmeister, 1994; Gendler et al., 2005). However, an alternative explanation may be the overlapping of two processes, namely the transformation of maghaemite (suggested above, first peak) and the Hopkinson peak, related to the wide grain size distribution of fine particles which undergo a transient SP phase during heating (second peak; the gradual increase of magnetic parameters from 400 °C followed by a drop from c. 500 to 580 °C; Muxworthy et al., 2002). Note that even when suitable fine-grained magnetite is present, the Hopkinson peak may be masked by coarser (MD) grains, abundant in analysed samples (see Figures 3 and 5), and result in flat insignificant thermal peaks (see Dunlop, 2014). The double peak (between ~300 and 500 °C) may also represent paramagnetic (i.e. phyllosilicates) mineral alteration during the heating cycle, as the clay mineral content varies from 10 to 40% within the PB section (Clarke et al., 2008). A small, hardly recognizable step-like feature or decay of magnetization appearing around 645 °C in the loess samples (LP: 36 and PB: 32) may indicate the T_C of thermally stable maghaemite (Gendler et al., 2005) (Figure 4a and b). The observed small peak between 650 and 700 °C on the heating curve of the PB170 sample (Fig. S3, PB170) can be defined as another Hopkinson peak related probably to secondary fine-grained haematite.

Discussion of AMS results and their environmental interpretation

We emphasize here that the inferences based on the AMS results are preliminary and should be further developed based on higher sampling resolution from both PB and LP. Nevertheless, the presented results are intended to facilitate an initial analysis of dominant patterns seen in the fabrics at these sites and assess the possibilities for palaeowind reconstructions from British loess.

The above magnetic investigation demonstrates that the predominant ferrimagnetic mineral in the sections is magnetite [i.e. in the LP section MD is dominant, while in the PB section PSD (mixed SD and MD) is dominant]. Therefore, the magnetic fabric is mainly controlled by MD grains, reflecting the shape-preferred orientation of the grains' alignment and thus yields a primarily oblate shape of the AMS ellipsoid (e.g. Hrouda, 1982). Notably, despite the presence of some SD magnetite grains, an inverse bulk AMS fabric (arising from crystallographically favoured alignment) was not predominantly preserved, although it did emerge as a secondary fabric resulting from sediment reworking (see' Site palaeoenvironmental comparison' below). The maximum susceptibility axes of primary fabrics are statistically well resolved at the specimen ($\varepsilon12 = 11.4 \pm 8.7°$) and population ($\varepsilon12 = 11.5°$) levels (see Table S1), and thus inferring palaeowind directions from the magnetic lineation appears possible. However, it is crucial to consider the impact of paramagnetic minerals, probably clay minerals, on the magnetic fabric record in this context (see e.g. Lagroix and Banerjee, 2002; Taylor and Lagroix, 2015; Bradák et al., 2018a). Based on the low magnetic susceptibility values observed in both analysed sections (κlf: $<5 \times 10^{-4}$ SI), and the lack of an apparent relationship between κlf and *Pj* (refer to Rochette, 1987; Hrouda and Jelínek, 1990; Rochette et al., 1992; Hus, 2003; Taylor and Lagroix, 2015; for more detailed information), it can be concluded that paramagnetic minerals do indeed make a substantial contribution to the magnetic fabric. Under prior research conducted by, for example, Taylor and Lagroix (2015), Lagroix and Borradaile (2000) and Költringer et al. (2021b), the AMS magnetic fabric of loess arises from the alignment of two components: the paramagnetic constituents (such as phyllosilicates, exhibiting an inherently oblate AMS character) and the ferrimagnetic minerals that are present to a lesser extent. Taylor and Lagroix (2015) suggest even that AMS is controlled by the paramagnetic mineral fraction rather than ferrimagnetic minerals. Nevertheless, even if the dominant magnetic carriers are clay minerals we can infer that the predominant sedimentary fabric remains intact in the sections, as oblate fabric is dominant in the bulk AMS results (Figure 6a–d). Below we discuss three possible interpretations of the AMS data, starting with consideration of possible past wind directions preserved in the fabric, and followed by analysis of possible complication factors such as slope deposition, and other post- or syn-depositional processes. We then consider the probable post-depositional origin of the nanofabric preserved in the fdAMS results.

Palaeowind reconstruction

Among the four studied horizons, the magnetic fabric of three units (both PB samples and LP20-2_1) shows quasi-horizontal foliation plains with different degrees of dip and lineation characteristics (Figure 6b–d). Well-defined lineation can be observed in LP20-2_1 (1 m depth), with a possible imbrication indicated by the discrepancy of the κ_{min} axis from vertical (Figure 6b). This type of loess magnetic fabric may suggest higher energy and relatively stable currents (wind) during deposition, as previously inferred from similar features observed in loess from the East European Plain and the Pannonian Basin by, for example, Nawrocki et al. (2006, 2019) and Bradák et al. (2020). In contrast, the magnetic fabric of both PB units probably indicates calmer sedimentary environments, evidenced by scattered lineation and a well-defined foliation plane (Figure 6c and d). These features probably reflect gravitation-controlled particle deposition, such as dust fall (see e.g. Bradák et al., 2020, and references therein). There are slight differences between the studied samples from the upper (PB160-170) and lower (PB240-245) units of the PB section (160–170 and 240-245 cm depths respectively; Figures 2 and 6c and d). The upper layer has less scattered and vertically oriented κ_{min} axes, while in the lower unit, the κ_{min} axes are tilted in a NW direction (Figure 6c and d).

Overall, the apparently well-preserved primary fabric of LP20-2_1 and the PB samples allows a preliminary examination of possible aeolian depositional processes. Under the model of Nawrocki et al. (2006), the orientation of κ_{max} axes shows the wind-driven direction of the magnetic lineation, the direction of which depends on wind strength. For weaker winds, the long axes of elongated grains are oriented parallel to the wind direction, while for stronger ones, the long axes are oriented perpendicular to the wind direction (see Tarling and Hrouda, 1993). Further, inclination of the foliation (tilting of κ_{min} axes) in this model is caused by the imbrication of platy minerals by a wind originating from the opposite direction as the dip. Thus, if the well-aligned, imbricated fabric of the lower sample from the LP site (LP20-2_1) is interpreted as reflecting wind directions under strong wind currents, as discussed above, then it may indicate SE winds during deposition. By contrast, if weaker winds are assumed, a SW direction would be reconstructed under this model. While the imbrication of κ_{min} axes does not allow testing between SE and SW winds in the lower LP sample, it does strongly support southerly blowing winds (Figure 6b). In turn, in the case of the PB site it is more difficult to define the characteristic flow directions during deposition, as κ_{max} axes are more randomly distributed along the bedding plane (Figure 6c and d), probably caused by lower transport energy (sedimentation rate is~40 cm ka^{-1} at c. 160 cm depth and <20 cm ka^{-1} PB at c. 240 cm depth; Stevens et al., 2020). Despite this, there is a slight tendency for grouping of κ_{max} axes in the S to SE direction for both layers (Figure 6c and d). However, for the upper PB sample the absence of imbrication of κ_{min} axes complicates interpretation of the wind direction, which can only be inferred from the κ_{max} distribution; as such, either southeasterly or northwesterly winds can be evoked, if weak wind is assumed (see Figure 6c). By contrast, in the lower PB layer the imbrication of κ_{min} axes to the NW suggests a dominant southeasterly wind direction (Figure 6d).

Although preliminary in nature, our results suggest that there is good reason to believe that reconstructions of past wind directions can be obtained from the AMS analysis of loess in southern England. The nature of prevailing dust-transporting winds in the English Channel area has previously been a source of considerable debate. Previous proposals include northerly, northeasterly or easterly, based dominantly on loess distribution, mineralogy and particle size (Figure 7; Catt, 1977; Catt et al., 1987; Lefort et al., 2011, 2013a; Stevens et al., 2020). This may reflect polar or ice sheet anticyclonic (Ludwig et al., 2016; Schaffernicht et al., 2020; see Figure 7a), Atlantic low-pressure system winds originating from depressions tracking to the south of the field area (Antoine et al., 2009; Pinto et al., 2020; Stevens et al., 2020; Figure 7b), or the

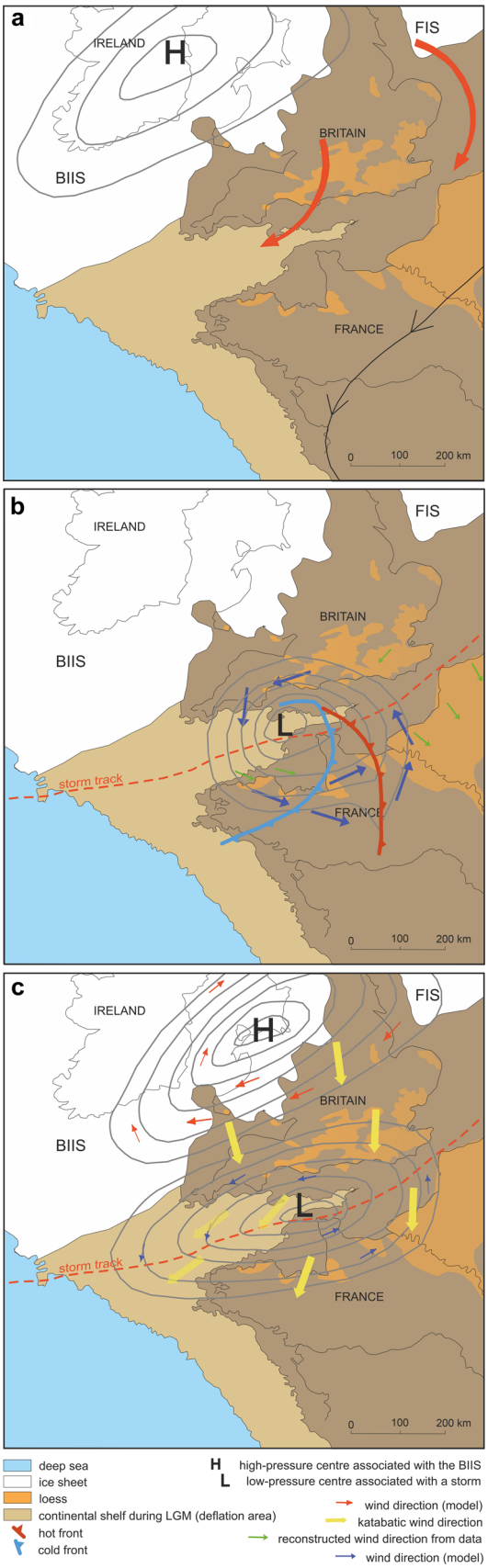

Figure 7. Three different scenarios of prevailing dust-transporting winds in the English Channel area around 21 ka: (A) high-pressure cell over the European Ice Sheet (EIS) and easterly winds (after Schaffernicht et al., 2020), (B) cyclones tracking over the channel (Antoine et al., 2009) and (C) katabatic winds (after Lefort et al., 2013a). Ice sheet extent after Clark et al. (2022) and loess distribution after Antoine et al. (2003). Abbreviations: British–Irish Ice Sheet (BIIS), Fennoscandian Ice Sheet (FIS). [Color figure can be viewed at wileyonlinelibrary.com]

influence of ice sheet katabatic winds (Lefort et al., 2013a; see Figure 7c). To date, published particle size and sediment source proxy data from LP are too limited to draw conclusions on dust sources and transport pathways at that site (although some evidence points to the influence of local sources having some influence along the south coast; see Bunce et al., 2022 for discussion). More detailed investigations have recently been conducted at PB, by Milodowski et al. (2015), Stevens et al. (2020) and Baykal et al. (2022), with a general consensus for relatively short-distance aeolian transport at the site, based on the mineralogy and coarse grain size of the sediments. However, while Milodowski et al. (2015) suggest some local bedrock contributions to dust sediment, Baykal et al. (2022) rule this out using a multi-proxy analysis of provenance indicators and demonstrate a dominantly BIIS source for loess at PB, with dust deflation from proximal glacial fluvial sediments in the exposed southern North Sea. Stevens et al. (2020) and Baykal et al. (2022) argue that the bulk of loess accumulated at PB occurs after the confluence of the BIIS and Fennoscandian Ice Sheet (FIS) after c. 26 ka, and continued broadly until the ice sheets decouple at c. 18 ka. This ice sheet coupling rerouted all ice sheet drainage into the southern North Sea and English Channel, and was probably coupled with a westward expansion of the Eurasian ice sheet high-pressure system, giving rise to robust north-easterly/easterly winds across southern Britain and the North Sea region (as detailed in Stevens et al., 2020). Alternatively, ice sheet katabatic winds (probably northerly to northeasterly) may have dominated at this time (Lefort et al., 2013a) or easterly flow associated with westerly tracking depressions south of the English Channel (Stevens et al., 2020). Considering AMS results, the change from stronger winds towards a calmer sedimentary environment as possible at PB may be linked to a change in atmospheric circulation. This would be consistent with the idea that the atmospheric constellation is greatly controlled by ice sheet extent, and the BIIS and FIS had separated and were decaying rapidly from around 20 ka (approximately the age of the upper PB sample). Under scenario A (Figure 7a) this would be consistent with a weaker high pressure over the ice sheet or that this high-pressure system was more over the FIS where the ice sheet was larger. Under scenario B (Figure 7b) this could indicate a change in the storm track related to a change in ice sheet extent (in particular the big Irish ice stream lobe was gone). In scenario C (Figure 7c) this would indicate less strong katabatic winds due to ice sheet extent.

Fully testing between these possibilities requires a more extensive AMS dataset than obtained here, but nonetheless, the interpretations outlined above allow a tentative suggestion of dominant southeasterly (or northwesterly) dust-transporting winds at the sites. Notably, this interpretation would argue against a katabatic origin for the dust-transporting winds, and rather points to influences from depressions tracking to the south of the site, or possibly an expanded ice sheet high-pressure system.

Deposition on a slope

It is important to highlight that when interpreting palaeowind direction based on AMS fabric, one must consider and rectify potential sources of misinterpretation, such as surface conditions during dust deposition, which may involve aspects such as inclination or palaeoslope. The magnetic fabric characteristics of slope sediments were originally described by Rees (1966) and later found in loess as well (e.g. Bradák et al., 2011; Bradák and Kovács, 2014). In the analysed samples, slope deposition may be indicated by the discrepancy of κ_{min} from

vertical (the dip of the foliation plane) and imbrication (Figure 6b and d). Such fabrics would indicate the possible dip and orientation of the slope, as the imbrication is in the same direction relative to the local surface of deposition (see e.g. Rees, 1966; Rees and Woodall, 1975; Ellwood and Howard, 1981). As such, an alternative interpretation of the magnetic fabric in at least the LP20-2_1 and the PB240-245 samples is that the material was deposited on a slope. Indeed, the interpretation of a trend to calmer wind regime during deposition of PB, as inferred from the changes in imbrication of κ_{min} in sample PB160-170 outlined above, would somewhat contradict previous suggestions that the upper unit may be the more reworked loess unit of the two (Milodowski et al., 2015; Stevens et al., 2020), and an alternative scenario may be that a stronger palaeoslope existed at the site during the earlier phases of loess deposition (c. 23–25 ka), and may have modified the contemporary dust fall, probably under periglacial conditions. Indeed, a related possibility is that following deposition, the material of LP20-2_1 and PB240-245 was redeposited by various surface processes, such as sheet-wash. In the case of LP20-2_1, the process might have re-aligned the original loess fabric and formed a strong lineation. Such a slope process would not have been as strong in the PB240-245 sample, as the lineation is less developed in this sample (Figure 6d).

In the case of PB240-245, a NW slope aspect would be inferred from the scattered distribution of κ_{min} (Figure 6). Indeed, the loess units at PB appear to gradually pinch out northeastward, due to the increasing elevation of the pre-Quaternary bedrock. However, if this exerted any influence on the imbrication it might be expected to do so via more southerly oriented slopes, and the underlying contact with the Thanet Formation at the PB is broadly flat (Murton et al., 2003). Irrespective, any potential palaeoslope might have been reduced by the time of the deposition of the younger unit at PB, as the dip in foliation is lower in that sample (Figure 6c; PB160-170). In turn, if slope-driven, the fabric of LP20-2_1 would point to deposition on a NE-facing slope (see Figure 6b). Although the Quaternary sediments here are underlain by a flat wave-cut gabbro platform, it is possible that loessic gelifluction deposits that directly underlie the loess may preserve a slope at the surface. However, the main headland adjacent to LP is oriented to the NW of the site, making a NE-facing slope unlikely.

As such, we suggest here that any interpretation of deposition or reworking on a slope and potential slope aspect does not precisely align with the frameworks presented by Rees (1966), Rees and Woodal (1975), or Ellwood and Howard (1981). According to these models, the inclination of κ_{min} should indicate the slope aspect, with κ_{max} axes primarily oriented in the same direction or perpendicular to it. However, the observed κ_{min} axes for both studied sites deviate considerably from this expectation, as any possible slope alignment at the sites predominantly opposes the inclination (as illustrated in Figure 6b and d). This inconsistency lends support to the notion of preserving a palaeowind record as a more plausible scenario, which is in line with the observations of, for example, Nawrocki et al. (2006; see 'Palaeowind reconstruction' above for details).

Pedogenic and other processes

Even though loess deposits can preserve the primary magnetic fabric originating from dust deposition, they can be easily altered by different secondary reworking processes, including pedogenesis, freeze–thaw and gelifluction (e.g. Bradák et al., 2020).

Based on the findings from Stevens et al. (2020), deposition of loess at PB occurs between ~16 and 26 ka. No recent age dating has been published at LP, but early luminescence ages also suggest peak last glacial age deposition (Wintle, 1981). Across western Europe, this timeframe aligns with the Upper Pleniglacial, representing the coldest period within the Weichselian glacial cycle. This period is characterized by ice expansion, widespread permafrost occurrence and substantial aeolian dust deposition, as documented by, among others, Vandenberghe and Pissart (1993), Antoine et al., (2001, 2009) and Guiter et al. (2003). Although there are compelling pieces of evidence indicating the presence of permafrost in western Europe during this time, Murton et al. (2003) only observed extensive solifluction and cryogenic features in underlying rocks and sediments in the Thanet area (PB), prior to loess accumulation. Nonetheless, the properties of the upper unit at PB and some fragipan-like features at LP have stimulated discussion as to possible cryogenic, permafrost or gelifluction processes affecting the loess at both sites (Ealey and James, 2011; Milodowski et al., 2015; Murton and Ballantyne, 2017; Stevens et al., 2020).

The disrupted and turbulent arrangement of magnetic particles in the LP20-2_06 sample (at a depth of 60 cm), characterized by a somewhat biaxial–oblate-like pattern, may point to the disruptive impact of secondary processes within the upper part of the LP profile (as depicted in Figure 6a). This could have been driven by pedogenesis (Bradák et al., 2011; Bradák et al., 2020), cryoturbation (as noted Taylor and Lagroix, 2015) and/or sheet wash processes (as proposed by Bradák et al., 2011; Bradák and Kovács, 2014). However, the scattered direction of the principal susceptibilities may also indicate bioturbation (Ellwood, 1984; Taylor and Lagroix, 2015). On the one hand, the geochemical proxies for weathering and pedogenic processes tend to indicate a relatively higher degree of these processes in the LP section and to a lesser extent in the upper part of the PB section (refer to Fig. S1 and 'Magnetic susceptibility, grain size and geochemistry by depth' in the Results). The particular sample from the upper LP site was extracted from a broadened, darker layer just below the topsoil in the LP20-2 profile (a layer that is ~45 cm thick in LP19; as shown in Figure 2), also pointing to possible pedogenic influences. However, the unevenly banded orange and brown loess unit from which the sample was taken may also have been affected by seasonal waterlogging during active layer thawing, resulting in varying redox states. Furthermore, as both κ_{min} and κ_{max} axes in bulk AMS are randomly distributed in the upper LP sample, this might imply the influence of cryogenic processes. Regardless, it is worth noting that secondary processes have substantially diminished the primary sedimentary fabric in the LP20-2_0.6 layer. The flip side of this though is that the visibly well-preserved aeolian dust fall fabric found in the upper sample from PB is unlikely to endure the active layer freeze–thaw processes as suggested by Stevens et al. (2020), nor the gelifluction suggested by Milodowski et al. (2015). This preservation is possibly more aligned with the upper unit's decalcification driven by soil formation processes, as discussed by Catt et al. (1987). Nonetheless, the impact of active layer processes on a flat loess surface on magnetic fabric needs more detailed study.

Frequency-dependent AMS results and origin of preserved 'nanofabric'

Evaluation of the allocation of the principal axis from fdAMS measurements, i.e. the orientation of the SP size nanoparticles, reveals similar results from the studied units (Figure 6e–h), even if the values of χFN are slightly higher in the PB section than in LP in the upper part (Figure 2). While the bulk fabric of

the upper LP sample (LP20-2_06) shows scattered alignment, an inverse nanofabric (sub-vertical orientation of SP grains) is preserved in the sample. Similarly, in the lower LP and upper PB units, despite the generally oblate AMS bulk fabric (Figure 6b and c), inverse (fdAMS) 'nanofabrics' can also be observed (Figure 6f and g).

Typically, this type of fabric in bulk AMS in rocks is caused by the 'single-domain effect' of magnetite (see e.g. Hrouda, 1982; Potter and Stephenson, 1988), but when applying fdAMS on loess samples, any signs of inversed fdAMS fabric have not been noticed, although some authors do not exclude the occurrence of possible partial inversion (e.g. Hrouda and Ježek, 2014; Bradák et al., 2018). Indeed, Hrouda and Ježek (2014) suggested the possibility of an unrecognized complexity in the particle-scale anisotropy of fdAMS. In any case, the sub-vertical orientation of SP grains (inverse fdAMS fabrics), deviating from the bedding plane (and sedimentary fabric), suggests the post-sedimentary formation of very fine magnetite grains oriented perpendicular to the bedding plane. One possible secondary process resulting in the neoformation of SP magnetite (characterized by inverse fdAMS) may be fine-grained downward mineral migration through percolation of water from the surface under wet conditions. This would have affected the whole LP section and at least the upper part of PB, while the lower PB unit nanofabric is more scattered (Figure 6h; PB240-245). This is in line with the greater current mean annual precipitation at the LP site compared to PB (c. 1000 to 600 mm at LP and PB respectively; Met Office UK). Another possibility may be preferential vertical orientation of SP grains during post-depositional soil formation under very wet conditions, although the exact mechanism for this is unclear. In any case, the occurrence of inversed fdAMS fabric in both, the upper PB layer, and LP layers, including the upper one with the heavily disrupted bulk fabric (Figure 6e–g), suggests that the neoformed nanofabric is significantly post-depositional, occurring after any cryoturbation, gelifuction or other reworkings that modified the upper LP layer (sample LP20-2_0.6). As such, these new observations of inversed nanofabric have great potential to reveal post-depositional processes occurring in loess.

Site palaeoenvironmental comparison – Environmental magnetic approach

Based on rock magnetism, AMS results and geochemical proxies it seems that the LP section is slightly more influenced by various post-depositional processes than the PB section (Table 1), including pedogenesis, cyclical variation in oxidation–reduction conditions and changes in hydrological conditions. The alterations in hydrological conditions, governed by either climatic shifts or changes in palaeotopography, could be regarded as a factor impacting both the magnetic fabric (see section above for details), but also the composition of magnetic minerals in the studied loess sections.

In many of the samples, weathering during early pedogenesis is probably a factor altering magnetic mineral composition, forming, for example, maghaemite. Indeed, the higher content of PSD grains in the PB section can be attributed to the presence of maghaemite (or magnetite with a high oxidation degree). Maghaemite can be abundant in palaeosols, as maghaemite also forms a transitional phase in a weathering sequence from ferrihydrite to haematite (Hao et al., 2009). Indeed, higher χlf and χFN values indicating *in situ* pedogenesis in the uppermost part of the sections broadly coincide with the observed Holocene soil (Figure 2), probably caused by the formation of new SP and SD magnetic minerals, presumably magnetite (as this process is well established by, for example, Zhou et al., 1990; Maher and Thompson, 1991; Heller et al., 1993). The slight offset of peak values to c. 30–40 cm below the surface in both sections is possibly a function of washing of the finest nanoparticles down profile under wet conditions, as potentially also hinted at by inverse nanofabrics (see Frequency-dependent AMS results and origin of preserved 'nanofabric' above).

Table 1. Summary of the magnetic mineralogy and AMS characteristics in the examined samples from both sites, Lowland Point (LP) and Pegwell Bay (PB), southern England.

Magnetic contributor	Magnetic characteristics		Comment
	LP section	PB section	
Domain characteristics	MD (mainly) + PSD (mixed SD & MD)	PSD (mixed SD & MD; mainly) + MD	Possible mixture of minerals with a sedimentary and post-depositional origin
Goethite	+	+ (sample PB 170)	**(1)** Sedimentary, detrital material from already weathered source **(2)** Neoformed during pedogenesis: temperature- and pH-sensitive goethite/haematite transformation; goethite prefers low tempertaure and pH
Maghaemite	+	++	(Grain surface) weathering, early pedogenic processes
Magnetite	+ MD + SD (Hopkinson, Verwey)	+ MD + SD (Hopkinson, Verwey)	Sedimentary (MD, SD) and secondary (e.g. pedogenic) origin (SD, SP)
Haematite	?	?	Very fine (SP) grains, if any Weathering: the cyclical appearance of oxidative/reductive environment; mainly pedogenic in origin, haematite prefers higher tempertaure and less humid conditions
AMS	Triaxial AMS ellipsoid, quasi-horizontal magnetic foliation	Oblate AMS ellipsoid, horizontal foliation	Primary depositional fabric preserved within a moderately compacted loess section
fdAMS	Inverse fabric	Inversed or scattered	**(1)** Inverse: post-depositional fabric of magnetite (vertically oriented SP grains) – the result of percolation (?) **(2)** Scattered – possible impact of the secondary process: hydrological, pedogenic and/or seasonal thawing

The presence of goethite within the LP section and at 170 cm depth in the PB section is notable and may indicate two contrasting scenarios: (i) differences in palaeoclimate conditions during pedogenic processes or (ii) variations in the source material of the deposited sediments. The formation of goethite and haematite in loess sections has been extensively studied, and it is well established that the haematite/(haematite + goethite) ratio indicates changes in specific pedoenvironmental conditions, such as shifts between colder or drier to warmer and/or humid, acidic and organically enriched conditions, in order to favour the prevalence of goethite over haematite (e.g. Schwertmann, 1985; Cornell and Schwertmann, 2003; Torrent et al., 2007). Consequently, the appearance of goethite in the LP loess section could be linked to the high precipitation into soils that are moderately drained. This conclusion is in line with the outcome from fdAMS, where inverse 'nanofabric' was observed (Figure 6e–h), suggesting the occurrence of processes producing and washing down, by, for example, percolation of water along the section, neoformed SP particles. It is also interesting to note that goethite-bearing bog iron has been found in a particularly marshy and waterlogged part of the loess outcrop, c. 50 m to the north of the LP20-2 section (Scott et al., 2011). This potentially supports the inference that waterlogging, which may also have occurred more widely at the site during periods of frozen ground, can drive goethite formation at the site. However, in contrast to this, following the research conducted by Torrent et al. (2006, 2007), a major contribution of goethite to loess may be that which formed in the source area prior to transport and deposition, with comparable concentrations in both the pedogenic and detrital fractions. Furthermore, the study by Hao et al. (2009) demonstrated that the goethite record predominantly reflects alterations in the source area preceding transportation and deposition, and might indicate progressive weathering in source regions. Indeed, goethite is a secondary weathering product of gabbroic rocks (Thompson and Rodgers, 1977), such as those underlying the LP site, potentially supporting the idea that local sources have some impact on the loess in Cornwall (Bunce et al., 2022).

In summary, post-depositional ferromagnetic minerals, including maghaemite and goethite, and hypothetically haematite (see Supporting Informatio, section 4), potentially provide insight into past environmental conditions or source areas. These post-depositional effects appear not to have altered the primary depositional (sedimentary) fabric resulting from palaeowind in at least three of the four AMS samples. Instead, all of these ferromagnetic minerals follow the original alignment of the sediments, which may support a detrital or early post-depositional origin for these minerals. By contrast, the fraction of the finest magnetic particles is oriented perpendicularly to the bedding plane and does not follow the alignment of the depositional fabric. A possible explanation for this is the influence of high levels of water percolation processes, probably during the Holocene, either aligning neoformed SP particles during soil formation with water flow downwards through the profile, or via the washing down of only the finest particles.

Conclusion

Mineral magnetic investigation of loess at opposite ends of a transect across southern England allows insight into the environmental processes during deposition at the end of the last glacial period (~25–18 ka), as well as post-depositional, Holocene, processes in southern England. First, the magnetic mineral composition was identified as broadly similar for both sites and originates from both sedimentary and post-depositional processes. Magnetite, derived from detrital input (MD, SD) and pedogenic origins (SD, SP), is the primary ferrimagnetic contributor. However, maghaemite resulting from weathering and/or early pedogenic processes is also prevalent. The presence of goethite in the LP section in Cornwall, western England, potentially indicates more pronounced weathering processes, although may reflect gabbro weathering in source rocks. Waterlogging at the LP section may have caused dissolution of fine magnetic minerals in the uppermost part of the section, potentially under seasonally thawed permafrost active layer conditions. Regardless, the main weathering imprint at the sections is Holocene in age.

Primary AMS fabrics are characterized by nearly vertical κ_{min} axes and horizontal magnetic foliations, aligning with the anticipated pattern for the deposition of silt-sized sediments onto a horizontally oriented bedding plane. While slight imbrications in lower samples at both sites may indicate deposition on a slope, we suggest the most plausible interpretation is that these minor imbrications are due to wind transport. The resulting tentative palaeowind reconstructions demonstrate higher energy and relatively stable wind during late last glacial loess deposition at the LP section (1 m depth). The prevailing wind direction at that time was SW or SE (the latter if a stronger wind is assumed) (Figure 6b). In contrast, the PB section is characterized by a generally calmer sedimentary environment, with dominant gravitational dust-fall deposition of loess. The palaeowind direction is interpreted to be broadly SE for both sampled layers (or NW for the upper PB layer, which shows no imbrication; Figure 6c), indicating a stable wind direction over several thousand years. On the other hand, post-depositional neoformation and/or transport of SP particles under intense water percolation conditions down section were identified within intervals having inverse fdAMS fabric. These magnetic fabrics are probably caused by processes associated with pedogenesis and percolation of water from the surface, aligning SP particles vertically, and probably occurred significantly post-depositionally, during Holocene conditions.

The reconstructed wind directions at the two sites in southern England contradict some previously presented models of dust-transporting winds in the region during the last glacial, notably the katabatic (northerly) model. However, we emphasize that these wind direction findings are preliminary. Most importantly, we demonstrate for the first time that primary depositional fabrics are preserved in loess in southern England and that these can be used for reconstructing past wind directions. Conducting systematic sampling for AMS investigations both vertically and spatially, particularly at the PB site, could yield valuable insights into the original air-fall fabric preserved in loess in southern England. This approach potentially allows robust reconstruction of wind directions in NW Europe during a highly dynamic phase of landscape and climate change.

Acknowledgments. This work was funded by the Swedish Research Council (VR grant 2017–03888) and the Quaternary Research Association (QRA) Quaternary Research Fund grants to T.S., as well as a grant from the Cornwall Area of Outstanding Natural Beauty. Ragna Orbe and James Gossip are thanked for help during field work and Charilaos Tsiavaras and Vanda Jakabova are thanked for preparing and analysing samples for grain size and X-ray fluorescence. Thanet District Council is thanked for site access at PB and Cornwall County Council and the National Trust are thanked for access at LP. Peter

Svedlindh is thanked for help with measurements at the Ångströmlaboratoriet, Uppsala University. D.K.N. was supported by the Polish National Agency for Academic Exchange no. BPN/BEK/2021/1/00221/U/00001, within the Bekker scholarship. The research was conducted with the institutional support RVO 67985831 of the Institute of Geology of the Czech Academy of Sciences.

Data availability statement

The data that supports the findings of this study are available in the supplementary material of this article

Supporting information

Additional supporting information can be found in the online version of this article.

Figure S1. Ratios of selected XRF results through the depth for the PB and LP sites. Abbreviations: Chemical Proxy of Alteration (CPA) – i.e. the molar ratio $Al_2O_3/(Al_2O_3 + Na_2O) \times 100$; ratio $(CaO^* + Na_2O + MgO)/TiO_2$ is a geochemical indicator of pedogenic intensity proposed by Yang et al. (2006), ratio $(CaO^* + Na_2O + MgO)/TiO_2$, a proxy Na_2O/Al_2O_3.

Figure S2. Characteristic types of heating and cooling curves from thermomagnetic experiments from pilot samples from LP (a to d plots) and PB (e to h plots) sites. The red curves indicate the heating and the blue curves the cooling steps.

Figure S3. Temperature dependence of magnetic susceptibility for selected samples from the PB and LP profiles. Data are normalized to the highest measured value. The red curves indicate the heating and the blue curves the cooling steps.

Figure S4. Field dependence of magnetic susceptibility (χ) at two operating frequencies (976 and 15,616 Hz) with frequency and field dependence parameters indicated for the low-frequency curves ($k_{HD} = 100 \times (\chi_{700} - \chi_{200})/\chi_{200}$ [%] where χ_{xxx} are magnetic susceptibilities in the respective field values). a) LP20-2_1 specimen, b) PB240-245 specimen.

Figure S5. The results of low-temperature magnetization experiments performed for representative specimens from Pegwell Bay (PB) from (a) 160 cm depth, (b) 240cm depth, and Lowland Point (LP) from (c) 60 cm and (d) 100 cm depths. The experimental sequence includes the following steps: (1) Room Temperature SIRM (RT-SIRM) which is the measurement of magnetization while cooling of the specimen from 300 to 10 K (from 26.85 to –263.15 °C) in 5 K intervals, (2) Low-Temperature SIRM (LT-SIRM) after the application of a 1 T field at 10 K (–263.15 °C), the field was switched off and the specimen was gradually heated to 300 K (26.85 °C), (3) Field Cooling (FC), entailing the measurement of magnetization during cooling in a continuous 1 T induced field, and (4) Zero Field Cooling (ZFC), involving magnetization measurement in zero magnetic fields in 10 K stages. Furthermore, selected specimens underwent initial heating to 400 K (126.85 °C) to eliminate potential goethite contributions, achieved by heating the samples above the Néel temperature of goethite (RT SIRM 300-400).

Table S1. Selected anisotropy parameters of magnetic susceptibility for all studied specimens from two sites in southern England: Pegwell Bay (PB) and Lowland Point (LP). The measurements were performed in a 200 A/m field and a frequency of 976 Hz. Abbreviations: L - lineation, F – foliation, P – degree of anisotropy, Pj - corrected degree of anisotropy of magnetic susceptibility, T – shape parameter, F-test, F12, F23, E12, E23, E13 - the parameters F-test for anisotropy, for explanation see the main text (section 3.1). Parameters that do not satisfy the statistical evaluation (F12 > 4°, ε12 < 20°, and F23 > 10°) are marked in red with a gray background, and these specimens were excluded from subsequent analysis.

Abbreviations. AMS, anisotropy of magnetic susceptibility; CIA, chemical index of alteration; LP, Lowland Point; LT-SIRM, low-temperature saturation isothermal remanent magnetization; MD, multi-domain; PB, Pegwell Bay; PSD, pseudo-single-domain; RT-SIRM, room-temperature saturation isothermal remanent magnetization; SD, single-domain; SP, superparamagnetic; χlf_{976}, low-frequency (976 Hz) magnetic susceptibility; χFN, Frequency-dependent magnetic susceptibility.

References

Antoine, P., Catt, J., Lautridou, J.-P. & Sommé, J. (2003) The loess and coversands of northern France and southern England. *Journal of Quaternary Science*, 18, 309–318. Available at: https://doi.org/10.1002/jqs.750

Antoine, P., Rousseau, D.D., Moine, O., Kunesch, S., Hatté, C., Lang, A. et al. (2009) Rapid and cyclic aeolian deposition during the Last Glacial in European loess: a high-resolution record from Nussloch, Germany. *Quaternary Science Reviews*, 28, 2955–2973.

Antoine, P., Rousseau, D.D., Zöller, L., Lang, A., Munaut, A.V., Hatté, C. et al. (2001) High-resolution record of the last interglacial-glacial cycle in the Nussloch loess-palaeosol sequences, Upper Rhine Area, Germany. *Quaternary International*, 76-77(77), 211–229.

Ao, H., Dekkers, M.J., Deng, C. & Zhu, R. (2009) Palaeoclimatic significance of the Xiantai fluvio-lacustrine sequence in the Nihewan Basin (North China), based on rock magnetic properties and clay mineralogy. *Geophysical Journal International*, 177, 913–924. Available at: https://doi.org/10.1111/j.1365-246X.2008.04082.x

Banerjee, S.K., Hunt, C.P. & Liu, X.-M. (1993) Separation of local signals from the regional paleomonsoon record of the Chinese loess plateau: a rock-magnetic approach. *Geophysical Research Letters*, 20, 843–846.

Bateman, R.M. & Catt, J.A., (2007) Provenance and palaeoenvironmental interpretation of superficial deposits, with particular reference to post-depositional modification of heavy mineral assemblages, Developments in Sedimentology, 58 (2007), pp. 151-188.

Baumgart, P., Hambach, U., Meszner, S. & Faust, D. (2013) An environmental magnetic fingerprint of periglacial loess: records of Late Pleistocene loess-palaeosol sequences from Eastern Germany. *Quaternary International*, 296(2013), 82–93. Available at: https://doi.org/10.1016/j.quaint.2012.12.021

Baykal, Y., Stevens, T., Bateman, M.D., Pfaff, K., Sechi, D., Banak, A. et al. (2022) Eurasian Ice Sheet derived meltwater pulses and their role in driving atmospheric dust activity: Late Quaternary loess sources in SE England. *Quaternary Science Reviews*, 296, 107804. Available at: https://doi.org/10.1016/j.quascirev.2022.107804

Borradaile, G. (1987) Anisotropy of magnetic susceptibility: rock composition versus strain. *Tectonophysics*, 138(2–4), 327–329 Available at: https://doi.org/10.1016/0040-1951(87)90051-5

Bradák, B. (2009) Application of anisotropy of magnetic susceptibility (AMS) for the determination of paleo-wind directions and paleo-environment during the accumulation period of Bag Tephra, Hungary. *Quaternary International*, 198(2009), 77–84. Available at: https://doi.org/10.1016/j.quaint.2007.11.005

Bradák, B. & Kovács, J. (2014) Quaternary surface processes indicated by the magnetic fabric of undisturbed, reworked and fine-layered loess in Hungary. *Quaternary International*, 319, 76–87. Available at: https://doi.org/10.1016/j.quaint.2013.02.009

Bradák, B., Seto, Y., Chadima, M., Kovács, J., Tanos, P., Újvári, G. et al. 2020. Magnetic fabric of loess and its significance in Pleistocene environment reconstructions. Earth-Science Reviews 210, November 2020, 103385. Available at: https://doi.org/10.1016/j.earscirev.2020.103385

Bradák, B., Seto, Y., Hyodo, M. & Szeberényi, J. (2018) Relevance of ultrafine grains in the magnetic fabric of paleosols. *Geoderma*, 330, 125–135. Available at: https://doi.org/10.1016/j.geoderma.2018.05.036

Bradák, B., Seto, Y., Stevens, T., Újvári, G., Fehér, K. & Költringer, C. (2021) Magnetic susceptibility in the European Loess Belt: new and existing models of magnetic enhancement in loess. *Palaeogeography, Palaeoclimatology, Palaeoecology*, 569, 110329. Available at: https://doi.org/10.1016/j.palaeo.2021.110329

Bradák, B., Thamó-Bozsó, E., Kovács, J., Márton, E., Csillag, G. & Horváth, E. (2011) Characteristics of Pleistocene climate cycles identified in Cérna Valley loess–paleosol section (Vértesacsa, Hungary). *Quaternary International*, 234, 86–97. Available at: https://doi.org/10.1016/j.quaint.2010.05.002

Bradák, B., Újvári, G., Seto, Y., Hyodo, M. & Végh, T. (2018) A conceptual magnetic fabric development model for the Paks loess in Hungary. *Aeolian Research*, 30(2018), 20–31.

Bradák, B., Újvari, G., Seto, Y., Hyodo, M. & Vegh, T. (2018a) A conceptual magnetic fabric development model for the Paks loess in Hungary. *Aeolian Res*, 30, 20e31. Available at: https://doi.org/10.1016/j.aeolia.2017.11.002

Budge, E. (1842) On the tract of land called the Lowlands in the Parish of St Keverne. *Transactions of the Royal Geological Society of Cornwall*, 6, 59–63.

Buggle, B., Glaser, B., Hambach, U., Gerasimenko, N. & Marković, S. (2011) An evaluation of geochemical weathering indices in loess–paleosol studies. *Quaternary International*, 240, 12–21. Available at: https://doi.org/10.1016/j.quaint.2010.07.019

Buggle, B., Hambach, U., Müller, K., Zöller, L., Marković, S.B. & Glaser, B. (2014) Iron mineralogical proxies and Quaternary climate change in SE-European loess–paleosol sequences. *CATENA*, 117, 4–22. Available at: https://doi.org/10.1016/j.catena.2013.06.012

Bunce, C., Smalley, I., Stevens, T. & Assadi-Langroudi, E. (2022) Loess in Britain and Ireland: Formation, modification and environmental significance, a review in memory of John Catt (1937–2017), Proceedings of the Geologists' Association, Volume 133, Issue 6, 501-517. Available at: https://doi.org/10.1016/j.pgeola.2022.06.005

Butcher, G.D.H. (1990) The magnetic fabric and depositional environments of loess deposits. University of Southampton, Doctoral Thesis.

Carter-Stiglitz, B.S., Moskowitz, B., Solheid, P., Berquo, T.S., Jackson, M. & Kosterov, A. (2006) Low-temperature magnetic behavior of multidomain titanomagnetites: TM0, TM16, and TM35. *Journal of Geophysical Research*, 111, B12S05. Available at: https://doi.org/10.1029/2006JB004561

Catt, J.A., Bateman, R.M., Wintle, A.G. & Murphy, C.P. (1987) The 'loess' section at Borden, Kent, S.E. England. *Journal of Quaternary Science*, 2(1987), 141–147.

Catt, J.A. (1977) Loess and coversands. In: Shotton, F.W., (Ed.) *British Quaternary Studies: Recent advances*. Clarendon Press Oxford. pp. 222–229.

Catt, J. A., & Staines, S. J. (1982). Loess in Cornwall. *Proceedings of the Ussher Society*, 5(3), 368–375.

Chlachula, J., Evans, M.E. & Rutter, N.W. (1998) A magnetic investigation of a Late Quaternary loess/palaeosol record in Siberia: magnetic investigation of loess/palaeosol, Siberia. *Geophysical Journal International*, 132(1998), 128–132. Available at: https://doi.org/10.1046/j.1365-246x.1998.00399.x

Clark, C.D., Ely, J.C., Hindmarsh, R.C.A., Bradley, S., Ignéczi, A., Fabel, D. et al. (2022) Growth and retreat of the last British–Irish Ice Sheet, 31 000 to 15 000 years ago: the BRITICE-CHRONO reconstruction. *Boreas*, 51, 699–758. Available at: https://doi.org/10.1111/bor.12594

Clarke, M.L., Milodowski, A.E., Bouch, J.E., Leng, M.J. & Northmore, K.J. (2007) New OSL dating of UK loess: indications of two phases of Late Glacial dust accretion in SE England and climate implications. *Journal of Quaternary Science*, 22, 361–371.

Clarke, M.L., Milodowski, A.E., Northmore, K.J., Leng, M.J. & Bouch, J.E. (2008) Reply: evidence for episodic dust accretion in SE England. *Journal of Quaternary Science*, 23, 307–308.

Cornell, R.M. & Schwertmann, U. (2003) *The Iron Oxides: Structure, Properties, Reactions, Occurrences and Uses*, second ed. Wiley-VCH. p. 664

Dawson, T. (2013) Land at West Camel Road, Queen, Camel, Somerset: Geophysical Survey (Magnetic) Report. Thames Valley Archaeological Services, Site Code QCS 13/155.

Day, R., Fuller, M. & Schmidt, V.A. (1977) Hysteresis properties of titanomagnetites: grain-size and compositional dependence. *Physics of the Earth and Planetary Interiors*, 13, 260–267.

Dearing, J.A., Dann, R.J.L., Hay, K., Lees, J.A., Loveland, P.J., Maher, B.A. et al. (1996) Frequency-dependent susceptibility measurements of environmental materials. *Geophysical Journal International*, 124, 228–240. Available at: https://doi.org/10.1111/j.1365-246X.1996.tb06366.x

Deng, C., Zhu, R., Jackson, M.J., Verosub, K.L. & Singer, M.J. (2001) Variability of the temperature-dependent susceptibility of the Holocene eolian deposits in the Chinese loess plateau: a pedogenesis indicator. *Physics and Chemistry of the Earth, Part A: Solid Earth and Geodesy*, 26(Issues 11–12), 873–878. Available at: https://doi.org/10.1016/S1464-1895(01)00135-1

Derbyshire, E. & Mellors, T.W. (1988) Geological and geotechnical characteristics of some loess and loessic soils from China and Britain: a comparison. *Engineering Geology*, 25(Issues 2–4), 135–175. Available at: https://doi.org/10.1016/0013-7952(88)90024-5

Dunlop, D.J. (2002) Theory and application of the Day plot (Mrs/Ms versus Hcr/Hc) 2. Application to data for rocks, sediments, and soils. *Journal of Geophysical Research: Solid Earth*, 107(No. B3), 2057. Available at: https://doi.org/10.1029/2001JB000487

Dunlop, D.J., (2014) High-temperature susceptibility of magnetite: a new pseudo-single-domain effect, Geophysical Journal International, Volume 199, Issue 2, November 2014, Pages 707–716. Available at: https://doi.org/10.1093/gji/ggu247

Dunlop, D.J. & Özdemir, Ö. (1997) *Rock Magnetism. Fundamentals and Frontiers, Cambridge Studies in Magnetism Series*. Cambridge, New York, Port Chester, Melbourne, Sydney: Cambridge University Press. p. 573.

Ealey, P.J. & James, H.C.L. (2008) Countybridge Quarry, the Lizard Peninsula. *Cornwall – historical and geological significance of an abandoned quarry, Geoscience in South-west England*, 11(2008), 22–26.

Ealey, P.J. & James, H.C.L., (2011) Loess of the Lizard Peninsula, Cornwall, SW Britain, Quaternary International, Volume 231, Issues 1–2, 55-61. Available at: https://doi.org/10.1016/j.quaint.2010.06.018.

Eden, D.N. (1980) The loess of north-east Essex, England. *Boreas*, 9(1980), 165–177.

Ellwood, B.B. (1984) Bioturbation; minimal effects on the magnetic fabric of some natural and experimental sediments. *Earth and Planetary Science Letters*, 67, 367–376.

Ellwood, B.B. & Howard, J.H. (1981) Magnetic fabric development in an experimentally produced barchan dune. *Journal of Sedimentology – Petrology*, 51, 97–100.

Gao, X., Hao, Q., Oldfield, F., Bloemendal, J., Deng, C., Wang, L. et al. (2019) New high-temperature dependence of magnetic susceptibility-based climofunction for quantifying paleoprecipitation from Chinese loess. *G-cubed*, 20, 4273–4291. Available at: https://doi.org/10.1029/2019GC008401

Gehring, A.U. & Hofmeister, A.M. (1994) The Transformation of Lepidocrocite During Heating: A Magnetic and Spectroscopic Study. *Clays and Clay Minerals*, 42, 409–415. Available at: https://doi.org/10.1346/CCMN.1994.0420405

Gendler, T.S., Shcherbakov, V.P., Dekkers, M.J., Gapeev, A.K., Gribov, S.K. & McClelland, E. (2005) The lepidocrocite–maghemite–haematite reaction chain—I. Acquisition of chemical remanent magnetization by maghemite, its magnetic properties and thermal stability. *Geophysical Journal International*, 160, 815–832. Available at: https://doi.org/10.1111/j.1365-246X.2005.02550.x

Guiter, F., Andrieu-Ponel, V., de Beaulieu, J.L., Cheddadi, R., Calvez, M., Ponel, P. et al. (2003) The last climatic cycles in western Europe: a comparison between long continuous lacustrine sequences from France and other terrestrial records. *Quaternary International*, 111(1), 59–74.

Haesaerts, P., Juvigné, E., Kuyl, O., Mücher, H. & Roebroeks, W. (1981) Compte rendu de l'excursion du 12 juin 1981, en Hesbaye et au Limbutg Néerlandais, consacrée à la chronostratigraphie des loess du Pléistocène supérieure. *Annales de la Societé Géologique de Belgique*, 104, 223–240.

Hao, Q., Oldfield, F., Bloemendal, J., Torrent, J. & Guo, Z. (2009) The record of changing hematite and goethite accumulation over the past 22 Myr on the Chinese Loess Plateau from magnetic measurements and diffuse reflectance spectroscopy. *Journal of Geophysical Research: Solid Earth*, 114, B12101. Available at: https://doi.org/10.1029/2009JB006604

Heller, F., Shen, C.D., Beer, J., Liu, X.M., Liu, T.S., Bronger, A. et al. (1993) Quantitative estimates of pedogenic ferromagnetic mineral formation in Chinese loess and palaeoclimatic implications. *Earth and Planetary Science Letters*, 114(2–3), 385–390. Available at: https://doi.org/10.1016/0012-821X(93)90038-B

Hrouda, F., (1982) Magnetic anisotropy of rock and its application in geology and geophysics, Geophys. Surv., 5 (1982), pp. 37-82.

Hrouda, F., Chlupáčová, M. & Mrázová, Š. (2006) Low-field variation of magnetic susceptibility as a tool for magnetic mineralogy of rocks, Physics of the Earth and Planetary Interiors. *Issues/National Council of State Boards of Nursing (U.S.)*, 154(3–4), 323–336. Available at: https://doi.org/10.1016/j.pepi.2005.09.013

Hrouda, F. & Jelínek, V. (1990) Resolution of ferrimagnetic and paramagnetic anisotropies in rocks, using combined low-field and high-field measurements. *Geophysical Journal International*, 103, 75–84. Available at: https://doi.org/10.1111/j.1365-246X.1990.tb01753.x

Hrouda, F. & Ježek, J. (2014) Frequency-dependent AMS of rocks: a tool for the investigation of the fabric of ultrafine magnetic particles. *Tectonophysics*, 629, 27–38. Available at: https://doi.org/10.1016/j.tecto.2014.01.040

Hus, J.J. (2003) The magnetic fabric of some loess/palaeosol deposits. *Physics and Chemistry of the Earth, Parts A/B/C*, 28, 689–699. Available at: https://doi.org/10.1016/S1474-7065(03)00128-1

Jackson, M., Moskowitz, B., Rosenbaum, J. & Kissel, C. (1998) Field-dependence of AC susceptibility in titanomagnetites. *Earth and Planetary Science Letters*, 157(3–4), 129–139. Available at: https://doi.org/10.1016/S0012-821X(98)00032-6

James, H.C.L. (2004) Evidence for the extent of permafrost activity in South-West England during the last cold stage. *Geoscience in South-west England*, 11(2004), 37–41.

Jelínek, V., (1977) The Statistical Theory of Measuring Anisotropy of Magnetic Susceptibility of Rocks and its Application. Gepfyzika, Brno, 88 p.

Jiang, Z., Liu, Q., Dekkers, M.J., Colombo, C., Yu, Y., Barrón, V. et al. (2014) Ferro and antiferromagnetism of ultrafine-grained hematite. *Geochemistry, Geophysics, Geosystems*, 15, 2699–2712. Available at: https://doi.org/10.1002/2014GC005377

Jin, C. & Liu, Q. (2010) Reliability of the natural remanent magnetization recorded in Chinese loess. *Journal of Geophysical Research: Solid Earth*, 115, B04103. Available at: https://doi.org/10.1029/2009JB006703

Kąkol, Z. & Honig, J.M. (1989) Influence of deviations from ideal stoichiometry on the anisotropy parameters of magnetite Fe3(1-δ) O4. *Physical Review B*, 40, 9090–9097.

Keen, D.H., Van Vliet-Lanoe, B. & Lautridou, J.P. (1996) Two long sedimentary records from Jersey, Channel Islands: stratigraphie and pedological evidence for environmental change during the last 200 kyr, Quaternaire, 7-1, pp. 3-13.

Kerney, M.P. (1965) Weichselian deposits of the Isle of Thanet, East Kent. PGA (Proc. Geol. Assoc.) 76, 269e274.

Költringer, C., Bradák, B., Stevens, T., Almqvist, B., Banak, A., Lindner, M. et al. (2021b) Palaeoenvironmental implications from Lower Volga loess - Joint magnetic fabric and multi-proxy analyses. *Quaternary Science Reviews*, 267, 107057. Available at: https://doi.org/10.1016/j.quascirev.2021.107057

Költringer, C., Stevens, T., Bradák, B., Almqvist, B., Kurbanov, R., Snowball, I. et al. (2021a) Enviromagnetic study of Late Quaternary environmental evolution in Lower Volga loess sequences Russia. *Quaternary Research*, 103, 49–73. Available at: https://doi.org/10.1017/qua.2020.73

Krs, M., Novák, F., Krsová, M., Pruner, P., Kouklíková, L. & Jansa, J. (1992) Magnetic properties and metastability of greigite-smythite mineralization in brown-coal basins of the Krušné hory Piedmont, Bohemia. *Physics of the Earth and Planetary Interiors*, 70, 273–287.

Lagroix, F. & Banerjee, S.K. (2002) Paleowind directions from the magnetic fabric of loess profiles in central Alaska. *Earth and Planetary Science Letters*, 195, 99–112. Available at: https://doi.org/10.1016/S0012-821X(01)00564-7

Lagroix, F. & Banerjee, S.K. (2004) The regional and temporal significance of primary aeolian magnetic fabrics preserved in Alaskan loess. *Earth and Planetary Science Letters*, 225(3–4), 379–395. Available at: https://doi.org/10.1016/j.epsl.2004.07.003

Lagroix, F. & Borradaile, G.J. (2000) Magnetic fabric interpretation complicated by inclusions in mafic silicates. *Tectonophysics*, 325(3), 207–225.

Lautridou, J.-P. (1985) Le cycle périglaciaire pléistocène en Europe du Nord-Quest et plus particulièrement en Normandie. *Centre Géom. édit.* 2, 908.

Lautridou, J.-P. & Sommé, J. (1974) Les loess et les provinces climato-sédimentaires du Pléistocène supérieur dans le Nord-Ouest de la France. Essai de corrélation entre le Nord et la Normandie. Quaternaire, 1974, 11-3-4, pp. 237-241.

Lefort, J.-P., Danukalova, G.A. & Monnier, J.L. (2011) Origin and emplacement of the loess deposited in northern Brittany and under the English Channel. *Quaternary International*, 240(Issues 1–2, 1), 117–127.

Lefort, J.-P., Monnier, J.-L. & Danukalova, G.A. (2013a) Deflation and transportation of the Upper Pleistocene Loess particles by katabatic winds during the lowstands of the English Channel: new data and new constrains. Contribution of the heavy minerals. In: Rădan, S., Rădan, S.-C. & Vasiliu, C. (eds) Correlations of quaternary fluvial, eolian and marine sequences. SEQS/INQUA Meeting, Constantsa, Romania. National Institute of Marine Geology and Geoecology, Bucharest, 25–26.

Lehmkuhl, F., Nett, J.J., Pötter, S., Schulte, P., Sprafke, T., Jary, Z. et al. (2021) Loess landscapes of Europe – Mapping, geomorphology, and zonal differentiation, Earth-Science Reviews, Volume 215, 2021, 103496. Available at: https://doi.org/10.1016/j.earscirev.2020.103496

Li, G., Xia, D., Appel, E., Wang, Y., Jia, J. & Yang, X. (2018) A paleomagnetic record in loess–paleosol sequences since late Pleistocene in the arid Central Asia. *Earth, Planets and Space*, 70, 44. Available at: https://doi.org/10.1186/s40623-018-0814-8

Liu, Q., Deng, C., Yu, Y., Torrent, J., Jackson, M.J., Banerjee, S.K. et al. (2005) Temperature dependence of magnetic susceptibility in an argon environment: implications for pedogenesis of Chinese loess/palaeosols. *Geophysical Journal International*, 161, 102–112. Available at: https://doi.org/10.1111/j.1365-246X.2005.02564.x

Liu, Q., Yu, Y., Torrent, J., Roberts, A.P., Pan, Y. & Zhu, R. (2006) Characteristic low-temperature magnetic properties of aluminous goethite [α-(Fe, Al)OOH] explained. *Journal of Geophysical Research: Solid Earth*, 111, B12S34. Available at: https://doi.org/10.1029/2006JB004560

Liu, X., Shaw, J., Jiang, J.Z., Bloemendal, J., Hesse, P., Rolph, T. et al. (2010) Analysis on variety and characteristics of maghemite. Science China. *Earth Sciences*, 53/1, 1–10. Available at: https://doi.org/10.1029/2002JB002264

Liu, X., Shaw, J., Liu, T., Heller, F. & Yuan, B. (1992) Magnetic mineralogy of Chinese loess and its significance. *Geophysical Journal International*, 108, 301–308. Available at: https://doi.org/10.1111/j.1365-246X.1992.tb00859.x

Ludwig, P., Schaffernicht, E.J., Shao, Y. & Pinto, J.G. (2016) Regional atmospheric circulation over Europe during the Last Glacial Maximum and its links to precipitation. *Journal of Geophysical Research: Atmospheres*, 121, 2130–2145. Available at: https://doi.org/10.1002/2015JD024444

Maher, B.A. & Thompson, R. (1991) Mineral magnetic record of the Chinese loess and paleosols. *Geology*, 19(1), 3. Available at: https://doi.org/10.1130/0091-7613(1991)019<0003:MMROTC>2.3.CO;2

Marković, S.B., Hambach, U., Stevens, T., Jovanović, M., O'hara-Dhand, K., Basarin, B. et al. (2012) Loess in the Vojvodina region (Northern Serbia): an essential link between European and Asian Pleistocene environments. *Netherlands Journal of Geosciences - Geologie en Mijnbouw*, 91(1-2), 173–188. Available at: https://doi.org/10.1017/S0016774600001578

Milodowski, A.E., Northmore, K.J., Kemp, S.J., Entwisle, D.C., Gunn, D.A., Jackson, P.D. et al. (2015) The mineralogy and fabric of 'Brickearths' in Kent, UK and their relationship to engineering behaviour. *Bulletin of Engineering Geology and the Environment*, 74, 1187–1211. Available at: https://doi.org/10.1007/s10064-014-0694-5

Moskowitz, B.M., Frankel, R.B. & Bazylinski, D.A. (1993) Rock magnetic criteria for the detection of biogenic magnetite. *Earth and Planetary Science Letters*, 120(3–4), 283–300. Available at: https://doi.org/10.1016/0012-821X(93)90245-5

Murton, J.A., Bateman, M.D., Baker, C.A., Knox, R. & Whiteman, C.A. (2003) The devensian periglacial record on Thanet, kent, UK. Permafr. Periglac. *Process*, 14, 217–246.

Murton, J.B. & Ballantyne, C.K. (2017) Periglacial and permafrost ground models for Great Britain. In J. S. Griffiths, & C. J. Martin (Eds.), Engineering Geology and Geomorphology of Glaciated and Periglaciated terrain. Geological Society. Engineering geology special publications, 28, 501–597.

Muxworthy, A.R., Schmidbauer, E. & Petersen, N. (2002) Magnetic properties and Mössbauer spectra of urban atmospheric particulate matter: A case study from Munich, Germany. *Geophysical Journal International*, 150, 558–570. Available at: https://doi.org/10.1046/j.1365-246X.2002.01725.x

Nawrocki, J., Bogucki, A.B., Gozhik, P., Łanczont, M., Pańczyk, M., Standzikowski, K. et al. (2019) Fluctuations of the Fennoscandian Ice Sheet recorded in the anisotropy of magnetic susceptibility of periglacial loess from Ukraine. Boreas, Vol. 48, pp. 940–952. https://doi.org/10.1111/bor.12400. ISSN 0300-9483

Nawrocki, J., Polechońska, O., Boguckij, A. & Łanczont, M. (2006) Palaeowind directions recorded in the youngest loess in Poland and western Ukraine as derived from anisotropy of magnetic susceptibility measurements. *Boreas*, 35, 266–271.

Necula, C., Dimofte, D. & Panaiotu, C. (2015) Rock magnetism of a loess-palaeosol sequence from the western Black Sea shore (Romania)*Geophysical Journal International*, 202, 1733–1748. Available at: https://doi.org/10.1093/gji/ggv250

Oches, E.A. & Banerjee, S.K. (1996) Rock-magnetic proxies of climate change from loess -paleosol sediments of the Czech Republic. *Studia Geophysica Et Geodaetica*, 40, 287–300. Available at: https://doi.org/10.1007/BF02300744

Özdemir, Ö. & Dunlop, D.J. (1996) Thermoremanence and Néel temperature of goethite. *Geophysical Research Letters*, 23(9), 921–924. Available at: https://doi.org/10.1029/96GL00904

Özdemir, Ö., Dunlop, D.J. & Moskowitz, B.M. (1993) The effect of oxidation on the Verwey transition in magnetite. *Geophysical Research Letters*, 20, 1671–1674.

Pan, Y.X., Zhu, R.X., Liu, Q.S., Guo, B., Yue, L.P. & Wu, H.N. (2002) Geomagnetic episodes of the last 1.2 Myr recorded in Chinese loess. *Geophysical Research Letters*, 29, 1282. Available at: https://doi.org/10.1029/2001GL014024

Passier, H.F. & Dekkers, M.J. (2002) Iron oxide formation in the active oxidation front above sapropel S1 in the eastern Mediterranean Sea as derived from low-temperature magnetism. *Geophysical Journal International*, 150(1), 230–240. Available at: https://doi.org/10.1046/j.1365-246X.2002.01704.x

Pinto, J.G. & Ludwig, P. (2020) Extratropical cyclones over the North Atlantic and western Europe during the Last Glacial Maximum and implications for proxy interpretation. *Climate of the Past*, 16, 611–626. Available at: https://doi.org/10.5194/cp-16-611-2020,2020

Pitcher, W.S., Shearman, D.J. & Pugh, D.C. (1954) The Loess of Pegwell Bay, Kent, and its Associated Frost Soils. *Geological Magazine*, 91, 308–314.

Potter, D.K. & Stephenson, A. (1988) Single-domain particles in rocks and magnpostdepositional history of a loess-paleosol sequence at Nussloch Germanyetic fabric analysis. *Geophysical Research Letters*, 15, 1097–1100.

Rees, A.I. (1966) The effect of depositional slopes on the anisotropy of magnetic susceptibility of laboratory deposited sands. *The Journal of Geology*, 74, 856–867. Available at: https://doi.org/10.1086/627216

Rees, A.I. & Woodall, W.A. (1975) The magnetic fabric of some laboratory-deposited sediments. *Earth and Planetary Science Letters*, 25, 121–130.

Roberts, A.P., Almeida, T.P., Church, N.S., Harrison, R.J., Heslop, D., Li, Y. et al. (2017) Resolving the origin of pseudo-single domain magnetic behavior. *Journal of Geophysical Research: Solid Earth*, 122, 9534–9558. Available at: https://doi.org/10.1002/2017JB014860

Roberts, M.C. (1985) The geomorphology and stratigraphy of the Lizard Loess in south Cornwall, England. *Boreas*, 14, 75–82. Available at: https://doi.org/10.1111/j.1502-3885.1985.tb00889.x

Rochette, P. (1987) Magnetic susceptibility of the rock matrix related to magnetic fabric studies. *Journal of Structural Geology*, 9, 1015–1020. Available at: https://doi.org/10.1016/0191-8141(87)90009-5

Rochette, P., Jackson, M. & Aubourg, C. (1992) Rock magnetism and the interpretation of anisotropy of magnetic susceptibility. *Reviews of Geophysics*, 30(3), 209–226. Available at: https://doi.org/10.1029/92RG00733

Rose, J., Lee, J.A., Kemp, R.A. & Harding, P.A. (2000) Palaeoclimate sedimentation and soil development during the Last Glacial Stage (Devensian), Heathrow Airport, London, UK. *Quaternary Science Reviews*, 19, 827–847.

Sagnotti, L. (2007) Iron Sulfides. In: Gubbins, D. & Herrero-Bervera, E. (Eds) *Encyclopedia of Geomagnetism and Paleomagnetism*. Dordrecht: Springer. Available at: https://doi.org/10.1007/978-1-4020-4423-6_160

Schaffernicht, E.J., Ludwig, P. & Shao, Y. (2020) Linkage between dust cycle and loess of the Last Glacial Maximum in Europe, Atmos. *Chemical Physics*, 20, 4969–4986. Available at: https://doi.org/10.5194/acp-20-4969-2020,2020

Schneider, J., de Wall, H., Kontny, A. & Bechstädt, T. (2004) Magnetic susceptibility variations in carbonates of the La Vid Group (Cantabrian Zone, NW-Spain) related to burial diagenesis. *Sedimentary Geology*, 166, 73–88. Available at: https://doi.org/10.1016/j.sedgeo.2003.11.016

Schwertmann, U. (1985) The effect of pedogenic environments on iron oxide minerals. *Adv. Soil Sci.* 1, 172–200.

Scott, P.W., Ealey, P.J. & Rollinson, G.K. (2011) Bog iron ore from Lowland Point, St Keverne, Lizard, Cornwall. *Geoscience in South-West England*, 12, 260–268.

Smalley, I., O'Hara-Dhand, K., Wint, J., Machalett, B., Jary, Z. & Jefferson, I. (2009) Rivers and loess: The significance of long river transportation in the complex event-sequence approach to loess deposit formation. *Quaternary International*, 198(1–2), 7–18. Available at: https://doi.org/10.1016/j.quaint.2008.06.009

Spassov, S., Heller, F., Kretzschmar, R., Evans, M.E., Yue, L.P. & Nourgaliev, D.K. (2003) Detrital and pedogenic magnetic mineral phases in the loess/palaeosol sequence at Lingtai (Central Chinese Loess Plateau). *Physics of the Earth and Planetary Interiors*, 140, 255–275.

Stevens, T. & Baykal, Y. (2021) Detrital zircon U-Pb ages and source of the late Palaeocene Thanet Formation, Kent, SE England, Proceedings of the Geologists' Association, Vol. 132, Issue 2, 240-248. Available at: https://doi.org/10.1016/j.pgeola.2021.01.003

Stevens, T., Sechi, D., Bradák, B., Orbe, R., Baykal, Y., Cossu, G. et al. (2020) Abrupt last glacial dust fall over southeast England associated with dynamics of the British-Irish ice sheet. *Quaternary Science Reviews*, 250, 106641. Available at: https://doi.org/10.1016/j.quascirev.2020.106641

Tarling, D.H. & Hrouda, F. (1993) *The Magnetic Anisotropy of Rocks*. London: Chapman & Hall.

Tauxe, L., Bertram, H.N. & Seberino, C. (2002) Physical interpretation of hysteresis loops: Micromagnetic modeling of fine particle magnetite. *Geochemistry, Geophysics, Geosystems*, 3(10), 1–22. Available at: https://doi.org/10.1029/2001GC000241

Taylor, S.N. & Lagroix, F. (2015) Magnetic anisotropy reveals the depositional and postdepositional history of a loess-paleosol sequence at Nussloch (Germany). *Journal of Geophysical Research: Solid Earth*, 120, 2859–2876. Available at: https://doi.org/10.1002/2014JB011803

Taylor, S.N., Lagroix, F., Rousseau, D.-D. & Antoine, P. (2014) Mineral magnetic characterization of the Upper Pleniglacial Nussloch loess sequence (Germany): an insight into local environmental processes. *Geophysical Journal International*, 199, 1463–1480. Available at: https://doi.org/10.1093/gji/ggu331

Thistlewood, L. & Jianzhong, S. (1991) A palaeomagnetic and mineral magnetic study of the loess sequence at Liujiapo, Xian, China. *Journal of Quaternary Science*, 6(1991), 13–26.

Thompson, R.C. & Rodgers, K.A. (1977) Laterization of the ultramafic-Gabbro Association at North Cape, Northernmost New Zealand. *Journal of the Royal Society of New Zealand*, 7(3), 347–377. Available at: https://doi.org/10.1080/03036758.1977.10419433

Torrent, J., Barrón, V. & Liu, Q. (2006) Magnetic enhancement is linked to and precedes hematite formation in aerobic soil. *Geophysical Research Letters*, 33, L02401. Available at: https://doi.org/10.1029/2005GL024818

Torrent, J., Liu, Q., Bloemendal, J. & Barrón, V. (2007) Magnetic Enhancement and Iron Oxides in the Upper Luochuan Loess–Paleosol Sequence, Chinese Loess Plateau. *Soil Science Society of America Journal*, 71, 1570–1578. Available at: https://doi.org/10.2136/sssaj2006.0328

Vandenberghe, J. & Nugteren, G. (2001) Rapid climatic changes recorded in loess successions. *Global and Planetary Change*, 28(1–4), 1–9. Available at: https://doi.org/10.1016/S0921-8181(00)00060-6

Vandenberghe, J. & Pissart, A. (1993) Permafrost changes in Europe during the Last Glacial. *Permafrost and Periglacial Processes*, 4(2), 121–135.

White, H.J.O. (1928) Geology of the country near Ramsgate and Dover. Mem. Geol. Surv. G.B., Sheets 274 and 290.

Wintle, A.G. (1981) Thermoluminescence dating of late Devensian loesses in southern England. Nature, 289, 479—480.

Worm, H.-U., Clark, D. & Dekkers, M.J. (1993) Magnetic susceptibility of pyrrhotite: grain size, field and frequency dependence. *Geophysical Journal International*, 114(1), 127–137. Available at: https://doi.org/10.1111/j.1365-246X.1993.tb01472.x

Yang, S., Ding, F. & Ding, Z. (2006) Pleistocene chemical weathering history of Asian arid and semi-arid regions recorded in loess deposits of China and Tajikistan. *Geochimica et Cosmochimica Acta*, 70(Issue 7), 1695–1709. Available at: https://doi.org/10.1016/j.gca.2005.12.012

Zhou, L., Oldfield, F., Wintle, A., Robinson, S.G. & Wang, J.T. (1990) Partly pedogenic origin of magnetic variations in Chinese loess. *Nature*, 346, 737–739. Available at: https://doi.org/10.1038/346737a0

Zhu, R., Liu, Q. & Jackson, M.J. (2004) Paleoenvironmental significance of the magnetic fabrics in Chinese loess-paleosols since the last interglacial (<130 ka). *Earth and Planetary Science Letters*, 221, 55–69. Available at: https://doi.org/10.1016/S0012-821X(04)00103-7